

SYNTHESIS AND CHARACTERIZATION OF PHENANTHRO-IMIDAZOLE
BASED CONJUGATED COPOLYMER FOR OPTOELECTRONIC
APPLICATIONS

A THESIS SUBMITTED TO
THE GRADUATE SCHOOL OF NATURAL AND APPLIED SCIENCES
OF
MIDDLE EAST TECHNICAL UNIVERSITY

BY

NIMA SOHRABNIA

IN PARTIAL FULFILLMENT OF THE REQUIREMENTS
FOR
THE DEGREE OF MASTER OF SCIENCE
IN
POLYMER SCIENCE AND TECHNOLOGY

AUGUST 2016

Approval of the thesis:
**SYNTHESIS AND CHARACTERIZATION OF
PHENANTHRO-IMIDAZOLE BASED CONJUGATED COPOLYMER FOR
OPTOELECTRONIC APPLICATIONS**

Submitted by **Nima Sohrabnia** in partial fulfillment of the requirements for the degree of **Master of Science in Polymer science and Technology Department, Middle East Technical University** to,

Prof. Dr. **Gülbin Dural Ünver**
Director, Graduate School of **Natural and Applied Sciences** _____

Prof. Dr. Necati Özkan
Head of Department, **Polymer Science and Technology** _____

Assoc. Prof. Dr. Ali Çırpan
Supervisor, **Department of Chemistry** _____

Assoc. Prof. Dr. H. Emrah Ünalın
Co-Supervisor, **Dept. of Metallurgical and Materials Eng., METU** _____

Examining Committee Members:

Prof. Dr. Levent Toppare
Chemistry Dept., METU _____

Assoc. Prof. Dr. Ali Çırpan
Chemistry Dept, METU _____

Assoc. Prof. Dr. İrem Erel Göktepe
Chemistry Dept, METU _____

Assoc. Prof. Dr. Yasemin Arslan Udum
Advanced Technologies Dept., Gazi University _____

Asst. Prof. Dr. Görkem Günbaş
Chemistry Dept, METU _____

Date: 24.08.2016

I hereby declare that all the information in this document has been obtained and presented in accordance with academic rules and ethical conduct. I also declare that, as required by these rules and conduct, I have fully cited and referenced all material and results that are not original to this work.

Name, Last Name:

Signature:

ABSTRACT

SYNTHESIS AND CHARACTERIZATION OF PHENANTHRO-IMIDAZOLE BASED CONJUGATED COPOLYMER FOR OPTOELECTRONIC APPLICATIONS

Sohrabnia, Nima

M.S., Department Polymer Science and Technology

Supervisor: Assoc. Prof. Dr. Ali Çırpan

Co-Supervisor: Assoc.Prof. Dr. H. Emrah Ünalın

August 2016, 68 pages

Benzodithiophene and flourene represent tremendous promise as donor moieties in donor-acceptor approach for optoelectronic applications. The strong intermolecular π - π stacking, coplanar and rigid structure as well as symmetric configuration of these moieties enhance charge mobility and reduce band gap when incorporate in back bone of polymer within pull and push system. In order to decrease angle torsion and adjusting the optoelectronic properties of polymers, chalcogenophenes utilize as bridge between donor and acceptor. In this study, three different phenanthro imidazole containing conjugated copolymers (**P1**,**P2** and **P3**) were synthesized using benzodithiophene and flourene via Suzuki and Stille condensation reactions. The structural characterizations of polymers were performed by NMR and the molecular weight of these polymers was measured via GPC. **P1** utilized as active layer in single layer organic light emitting diode with device structure of ITO/PEDOT:PSS/**P1**/LiF:Al. The observed color was cyan with luminance of 5560

cd/m² at 13 volts. For photovoltaic application **P2** and **P3** were used as active layer with device structure of ITO/PEDOT:PSS/Polymer:PC₇₁BM/Ca:Al. The best of OPVs devices showed 0.94% PCE for **P2** and 0.91% for **P3** under standard AM 1.5 (100 mW/cm²) condition.

ÖZ

OPTOELEKTRONİK UYGULAMALAR İÇİN FENANTREN-İMİDAZOL İÇEREN KONJÜGE KOPOLİMERLERİN SENTEZİ VE KARAKTERİZASYONU

Sohrabnia, Nima

Yüksek Lisans, Polimer Bilim Ve Teknolojisi

Tez Yöneticisi: Doç. Dr. Ali Çırpan

Ortak Tez Yöneticisi: Doç. Dr. H. Emrah Ünalın

Ağustos 2016, 68 sayfa

Benzoditiyofen ve fluoren sahip olukları donör gruplarından dolayı optoelektronik uygulamalar için çok büyük umut vaad etmektedirler. Bu donör grupların sahip olduğu güçlü moleküler arası π - π dizinimi, eşdüzleme sahip olmaları, kararlı yapıları ve simetrik dizilişlerinden dolayı yük akışını arttırmaları. Ayrıca bu gruplar polimerin ana zincirinde bulduklarında band aralığını düşürme özelliğine sahiptir. Polimerlerin açılal bükülmesini ve optoelektronik özelliklerini arttırmak için beş halkalı köprüler alıcı ve verici guruplar arasında köprü olarak kullanılırlar. Bu çalışmada fenantren -imidazol içeren üç farklı konjuge kopolimer Suzuki ve Stille kenetlenme reaksiyonları ile gerçekleştirildi. Elde edilen polimerlerin yapısal karakterizasyonu Nükleer Manyetik Rezonans (NMR) ile yapıldı ve polimerlerin moleküler ağırlıkları Jel Süzölmeli Kromatografı (GPC) kullanılarak belirlendi. **P1** tek tabaka olarak, ITO/PEDOT: PSS/**P1**/LiF:Al OLED cihaz yapısında aktif tabaka olarak kullanıldı. Cam göbeği rengi yayan cihazın luminans değeri ise 13 Volt da 5560 cd/m² olarak ölçöldü. ITO/PEDOT: PSS/Polymer: PC₇₁BM/Ca:Al cihaz

yapısında **P2** ve **P3** aktif tabakada kullanıldılar. AM 1.5 (100 mW/cm²) şartları altında yapılan ölçümlerde, en iyi organik güneş pili sonuçları **P2** için % 0.94 PCE, **P3** için ise % 0.91 PCE şeklindedir.

To my gracious mother and altruist brother

ACKNOWLEDGEMENTS

I would like to indicate my extreme gratitude to my thesis supervisor Assoc. Prof. Ali ırpan. I owe thanks to him for endless efforts, precious feedback, patience and encouragements during my thesis study. Also, I will not forget insight and constructive criticism of Prof. Dr. Levent Toppare throughout in this study. Besides, I am so grateful of my co-supervisor Assoc. Prof. Dr. H. Emrah Ünalın for his guidance.

I express many thanks to my friends in ırpan Research Group. My special thanks go to Şevki Can Cevher, Gönül Hızalan, Şerife Özdemir Hacıođlu and Fatma Demir helping during this study. During this research also students Emre Ataođlu, Ipek Önk, Ece Aktaş, Duygu Keleş and Özge Karagacti provided a great encourage, comments and support to make this thesis as good as possible.

I am also indebted my lifelong friends Payam and Poorya Parvizi, Arif Badem, Muzafer Gencay Celik and Ali Gharibdoost for their endless support, especially during my thesis preparation.

My genuine appreciation goes to my amazing family members, my merciful Mom, my gentle dad (R.I.P.) and my generous brother who always got my back in ups and downs of life.

TABLE OF CONTENTS

ABSTRACT.....	v
ÖZ.....	vii
ACKNOWLEDGEMENTS.....	x
TABLE OF CONTENTS.....	xi
LIST OF TABLES.....	xiv
LIST OF FIGURES.....	xv
LIST OF ABBREVIATIONS.....	xviii
CHAPTERS	
1.INTRODUCTION.....	1
1.1 SEMICONDUCTORS.....	1
1.1.1 Application of Semiconductors.....	2
1.1.2 Photovoltaics.....	2
1.1.2.1 Inorganic Photovoltaics.....	2
1.1.2.2 Organic Photovoltaics.....	3
1.1.3 Light Emitting Diodes.....	4
1.1.3.1 Inorganic Light Emitting Diodes.....	4
1.1.3.2 Organic Light Emitting Diodes:.....	4
1.1.4 Electrochromic devices.....	5
1.2 CONJUGATED POLYMERS:.....	7
1.2.1 Band Gap Engineering.....	9
1.3 ORGANIC PHOTOVOLTAICS.....	10
1.3.1 Toward High Performance OPVs:.....	14
1.3.1.1 Donor Acceptor Approach.....	15
1.3.1.2 Narrow Band Gap:.....	16
1.3.1.3 Morphology Optimization:.....	16

1.3.2 Characterization of OPVs.....	17
1.3.2.1 Short Circuit Current Density	17
1.3.2.2 Open Circuit Voltage	17
1.3.2.3 Equivalent Circuit	19
1.3.2.4 Fill Factor and Power Conversion Efficiency	20
1.4 ORGANIC LIGHT EMITTING DIODE	21
1.4.1 White Organic Light Emitting Diodes:	23
1.4.2 Color Quality of Polymer Light-Emitting Devices	24
1.4.3 Characterization of Polymer Light-Emitting Devices.....	25
1.5 MOTIVATION OF STUDY	25
2.EXPERIMENTAL	29
2.1 MATERIALS	29
2.2 INSTRUMENTATION.....	29
2.2.1 Electrochemical Studies	29
2.2.2 Spectroelectrochemical Studies.....	30
2.2.3 Kinetic Studies	30
2.2.4 Thermal Analysis	30
2.2.5 Gel Permeation Chromatography.....	31
2.3 SYNTHESIS OF 2,5-DIBROMOTHIOPHENE-3-CARBALDEHYDE	31
2.8 SYNTHESIS OF 2-(2,5-DIBROMOTHIOPHEN-3YL)-1-(4-HEXYLPHENYL)-1H-PHENANTHRO[9,10-D]IMIDAZOLE.....	32
2.9 SYNTHESIS OF 2-(2,5-DIBROMOTHIOPHEN-3-YL)-1-(4-FLUOROPHENYL)-1H-PHENANTHRO[9,10-D]IMIDAZOLE.....	33
2.10 SYNTHESIS OF TRIBUTYL(4-HEXYLTHIOPHEN-2-YL)STANNANE.....	34
2.11 SYNTHESIS OF 2-(4,4"-DIHEXYL-[2,2':5',2"-TERTHIOPHEN]-3'-YL)-1-(4-FLUOROPHENYL)-1H-PHENANTHRO[9,10-D]IMIDAZOLE	34
2.12 SYNTHESIS OF 2-(5,5"-DIBROMO-4,4"-DIHEXYL-[2,2':5',2"-TERTHIOPHEN]-3'-YL)-1-(4-FLUOROPHENYL)-1H-PHENANTHRO[9,10-D]IMIDAZOLE.....	35
2.13 SYNTHESIS OF P1	36
2.14 SYNTHESIS OF P2.....	37

2.15 SYNTHESIS OF P3.....	38
2.16 ORGANIC PHOTOVOLTAIC DEVICE FABRICATION.....	39
2.17 OLED DEVICE FABRICATION.....	40
3.Results and discussion	41
3.1 SYNTHESIS	41
3.2 CYCLIC VOLTAMMETRY	42
3.3 SPECTROELECTROCHEMICAL STUDIES	44
3.4 KINETIC STUDIES	45
3.5 OPTICAL PROPERTIES OF POLYMERS	47
3.6 THERMAL ANALYSIS OF POLYMERS	48
3.7 POLYMER LIGHT EMITTING DIODE APPLICATION OF P1	49
3.8 ORGANIC PHOTOVOLTAIC APPLICATION	51
4.Conclusion	55
REFERENCES	57
APPENDIX A.....	61
NMR RESULTS	61
APPENDIX B.....	67
THERMAL ANALYSIS RESULTS.....	67

LIST OF TABLES

Tables

Table 1. Electrochemical Characteristics of P3	44
Table 2. Switching Times and Optical Contrast in Near IR and Visible region	46
Table 3. Optical Properties of Polymer.	48
Table 4. Optimization Studies of P2 and P3 for OPVs.	53

LIST OF FIGURES

Figures

Figure 1. Schematic Presentation of intersoliton hopping.	8
Figure 2. Band Gap Diagram.	9
Figure 3. a) Resonance Structure of Polymers. b) Factor Effecting Band gap	10
Figure 4. Conjugated Polymer P3HT as the Donor and PCBM as the Acceptor.....	11
Figure 5. The Structure of the Polymer That Shows Highest PCE Performed Polymer in Literature.	12
Figure 6. Working principle of an OPV	12
Figure 7. Foster and Dexter Energy Transfer.....	13
Figure 8. a) Donor and Acceptor Approach b) Hybridization resulting from D-A approach c) Donor or Acceptor Moieties reproduced from[23]	15
Figure 9. Solar Spectrum in 1.5 G Condition Reproduced From [33].....	16
Figure 10. Equivalent Circuit of Organic Semiconductors Reproduced From [39]	19
Figure 11. The Fill Factor and an Ideal cell Fill Factor reproduced from [23].....	21
Figure 12. Working Principle of OLED.....	22
Figure 13. Single Layer OLED Device structure.....	22
Figure 14. Fluorescence and Phosphorescence radiative decay.....	23
Figure 15. Corresponding Angle of Phenanthroimidazole derivative of thiophene reproduced from [47]	26
Figure 16. Structure of the Polymers.	28
Figure 17. Synthesis of 2,5-dibromothiophene-3-carbaldehyde	31
Figure 18. Synthesis of 2-(2,5-dibromothiophen-3-yl)-1-(4-hexylphenyl)-1H-phenanthro[9,10-d]imidazole	32
Figure 19. Synthesis of 2-(2,5-dibromothiophen-3-yl)-1-(4-fluorophenyl)-1H-phenanthro[9,10-d]imidazole	33
Figure 20. Synthesis of tributyl(4-hexylthiophen-2-yl)stannane	34
Figure 21. Synthesis of 2-(4,4"-dihexyl-[2,2':5',2"-terthiophen]-3'-yl)-1-(4-fluorophenyl)-1H-phenanthro[9,10-d]imidazole	34

Figure 22. Synthesis of 2-(5,5"-dibromo-4,4"-dihexyl-[2,2':5',2"-terthiophen]-3'-yl)-1-(4-fluorophenyl)-1H-phenanthro[9,10-d]imidazole.....	35
Figure 23. Synthesis of P1.....	36
Figure 24. Synthesis of P2.....	37
Figure 25. Synthesis of P3.....	38
Figure 26. Cyclic Voltammetry of P1, P2 and P3	43
Figure 27. Spectroelectrochemical Spectra of P3 and color at -2, 0, 1 and 1.1 V.	45
Figure 28. Percent Transmittance Change of P3	46
Figure 29. Uv-Visible Absorption Spectra of the Polymers (P1 , P2 and P3) in chloroform Solution and thin film.....	48
Figure 30. Photoluminescence of P1 in chloroform solution and thin film.	49
Figure 31. P1 . JLV Characteristics of P1 with Maximum Luminescence at 13 V and 1267 mA/cm ²	50
Figure 32. The Electroluminescence of P1 at 12 V and maximum emission of 476 nm.....	50
Figure 33. Color Coordinates of Emitted Light by P1	51
Figure 34. J-V characteristics of P2 and P3	52
Figure 35. ¹ H NMR of 2,5-dibromothiophene-3-carbaldehyde	61
Figure 36. ¹ H NMR of 2-(2,5-dibromothiophen-3-yl)-1-(4-hexylphenyl)-1H-phenanthro[9,10-d]imidazole	61
Figure 37. ¹³ C NMR of of 2-(2,5-dibromothiophen-3-yl)-1-(4-hexylphenyl)-1H-phenanthro[9,10-d]imidazole	62
Figure 38. ¹ H NMR of 2-(2,5-dibromothiophen-3-yl)-1-(4-fluorophenyl)-1H-phenanthro[9,10-d]imidazole	62
Figure 39. ¹³ C NMR of of 2-(2,5-dibromothiophen-3-yl)-1-(4-fluorophenyl)-1H-phenanthro[9,10-d]imidazole	63
Figure 40. ¹ H NMR of 2-(4,4"-dihexyl-[2,2':5',2"-terthiophen]-3'-yl)-1-(4-fluorophenyl)-1H-phenanthro[9,10-d]imidazole.....	63
Figure 41. ¹ H NMR of 2-(5,5"-dibromo-4,4"-dihexyl-[2,2':5',2"-terthiophen]-3'-yl)-1-(4-fluorophenyl)-1H-phenanthro[9,10-d]imidazole.....	64

Figure 42. ^{13}C NMR of 2-(5,5''-dibromo-4,4''-dihexyl-[2,2':5',2''-terthiophen]-3'-yl)-1-(4-fluorophenyl)-1H-phenanthro[9,10-d]imidazole.	64
Figure 43. ^1H NMR of P1.	65
Figure 44. ^1H NMR of P2.	65
Figure 45. ^1H NMR of P3.	66
Figure 46. DSC Thermogram of P1	67
Figure 47. DSC Themogram of P2	67
Figure 48. TGA Curve of P1	68
Figure 49. TGA Curve of P2	68

LIST OF ABBREVIATIONS

CE	Coloration Efficiency
OD	Optical Density
BLA	Bond Length Alternation
PEDOT	Poly (3, 4-ethylenedioxythiophene)
PV	Photovoltaic
OPV	Organic Photovoltaic
LED	Light Emitting Diode
OLED	Organic Light Emitting Diode
ITO	Indium Tin Oxide
PCE	Power conversion Efficiency
FRET	Förster Resonant Energy Transfer
LUMO	Lowest Occupied Molecular Orbital
HOMO	Highest Occupied Molecular Orbital
E_g	Band Gap
QE	Quantum Efficiency
LE	Luminous Efficiency
J_{sc}	Short Circuit Current Density
EQE	External Quantum Efficiency
FF	Fill Factor
DSC	Differential Scanning Calorimeter
TGA	Thermo Gravimetric Analysis
RGB	Red, Green and Blue
LI	Luminous Intensity
HTL	Hole Transport Layer
JLV	Current Density-Luminesce-Voltage
BDT	Benzodithiophene
ECD	Electrochromic device

CHAPTER 1

INTRODUCTION

1.1 Semiconductors

The useful way to describe conduction in materials is band gap theory. In this theory, materials can be divided into three major class on basis of conduction. These are the conductors (such as metals), insulator (such as saturated plastics) and semiconductors. In conductors, the conduction band and valance band are overlap, hence, electron can move freely in these materials. On the other hand, in insulators the electron could not move in martials because large band gap (larger than 5 eV). Semiconductors have band gap about 0.5-4.5 eV. Because of relatively smaller bad gap, electrons can move to conduction band in certain condition. For example, under illumination of light electrons exited and can move. Semiconducting materials can be divided into two main group. The pioneer class of semiconductors are based on inorganic materials whereas the new generation one is organic semiconductors. One of the difference of these materials is the charge transfer mechanism. In inorganic materials the drift and diffusion of the charge is main reason for charge transport. However, in organic materials the hoping of electron to the empty state is the main reason for charge transport. Another difference is their dielectric constant. Organic materials have smaller dielectric constant result in formation of exitons with relatively high columbic interaction compare to inorganic materials. This means the charge separation in organic materials is more vital. To overcome this problem donor acceptor molecule is utilized in organic materials.

1.1.1 Application of Semiconductors

The key concept in optoelectronic devices is the interchangeable transformation between light and electricity which depends on interaction of electrons and light within semiconductors. The band gap of semiconducting material is crucial for desired application. By tuning the band gap of semiconductors, their properties can be tailored from insulator to conductive materials. Electrochromic devices (ECDs), Light Emitting Diodes (LEDs), Field Effect Transistors (FETs) and Photovoltaics (PVs) are well-known examples of optoelectronic devices. The semiconductors generally can be categorized as organic and inorganic. Inorganic ones have been utilized in almost all electronic devices from early 20 centuries. However, the new area in semiconductors emerged in the last 3 decades based on organic materials. During these 30 years many efforts have been done to improve performance of these devices. One of the promising approach is utilizing organic macromolecule, in other words, conjugated polymers. The focus of this work is to synthesize novel conjugated polymers for Organic Photovoltaics (OPV) and organic light emitting diode OLED applications. In upcoming section of this chapter descriptions are given to understand the difference between organics and inorganics in terms of performance and engineering point of view. In sections (2,3 and 4) of this chapter a great discussion on conjugated polymers; OPVs and OLEDs will be reviewed.

1.1.2 Photovoltaics

As the demand for renewable energy considering the limitations and disadvantages of traditional fuels, photovoltaic (PV) cells have become a center of great attention. These are semiconductors that output current directly from light. Records show Alexandre Edmund Becquerel's efforts and observations in obtaining current from applying light to electrochemical cells in 1839 that actually pioneered this interesting field.

1.1.2.1 Inorganic Photovoltaics

Although today, silicon based solar cells which constitute 90% of solar energy

produced all over the world have an efficiency of 25.6% using single crystal materials and 21.3 % using the polycrystalline [1]. In fact, it was as low as 4% which is a clear implication of advancement in the field [2]. Efficiency is dependent on band gap (E_g) which is 1.1 eV in silicon where band gap for utmost quantum efficiency (QE) for a single crystal is 1.3 eV, silicon has obtained great amount of attention and significance. However, there are alternatives to this single crystal silicon solar cells which reduce the manufacturing cost [1]. Nevertheless, advanced multi-junction devices are produced which yields efficiency of up to 46.7 % based on these materials. These devices show promising power conversion efficiency (PCE) due to their high mobility of free carriers, high current density and high internal quantum efficiency [3]. On the other hand, there are some problems with the devices, most challenging of which are impossibility of integration onto flexible substrates in crystal form and high production cost arising from the demand for high temperature for integration of materials. As long as low-cost and high-efficiency are concerned, researchers put their research focus on production thin layer, effective way to purification of silicon and other alternative materials such as organic compounds.

1.1.2.2 Organic Photovoltaics

To attack the problem associated with the manufacturing of optoelectronic devices, organic semiconductors including both polymers and small molecules are being used widely. Having π -electron delocalization on their backbone, these molecules exhibit certain conductivity features through intermolecular or intramolecular bonds. The range of the energy gap in organic semiconductors is between 1.4-3.0 eV for absorption in visible region and absorption to Near-IR region which enhance the performance of organic photovoltaics [4]. Studies continue to increase the efficiency and there has been developments from 1% to 11.7% nowadays [5]. Solution processable conjugated polymers and thermally deposited small molecules are used in manufacturing of organic photovoltaics. Since they show strong absorption properties, the ease in purification and the possibility of being deposited onto flexible substrates at low cost, polymers become center of consideration in applications related to OPV and OLED [6].

1.1.3 Light Emitting Diodes

Considering the fact that nearly one-fifth of the global electricity consumption is due to lightning and great portion of it is wasted as heat rather than light, calls for determined investigation of light bulbs. Toward resolving this issue, substitution of Compact Fluorescent Lights for incandescent was the first step however, so far the best solution happen to be LED usage of which is expected to greatly expand in the coming few years.

1.1.3.1 Inorganic Light Emitting Diodes

The first known LED dates back in early 20th century when H. J. Round found the first one in 1907. However, it was commercialized after discovery of Holonyak (Galium, Arsenic and Phosphorous); a red emitting LED. The white color was achieved by stacking primary colors (red, green and blue) which have been used as solid state lightning.

1.1.3.2 Organic Light Emitting Diodes:

Pope and coworkers reported the first electroluminescence from organic solids composed of anthracene [7]. Nevertheless, it was Vincett's effort of depositing amorphous thin films of anthracene using vacuum sublimation that caused voltage drop indicating the viability of vacuum sublimation method of small molecular organic LED devices' production. The first polymer LED in which a precursor polymer was spin cased onto Indium Tin Oxide (ITO) coated glass was brought about by Friend and constituents after achievements in fabrication of small molecular OLEDs in 1990 [8]. Besides, in polymer based LED molecules covalently bonded to each other and chains have van der waals interaction which increase the mechanical properties of device. The solubility of polymers allows them to easily processing specially for mass production via spin coating or inkjet printing. Other remarkable advantages of OLEDs are full angle viewing, possibility of flexible display depending on flexible coatings, high efficiency and many more to be explored.

1.1.4 Electrochromic devices

The reversible capability of material to alter its color depending on the potential applied is called electrochromism and three types of them are known as inorganic materials, organic small molecules and conjugated polymers [9]. Smart windows, display panels and smart mirrors are some of the application areas of ECDs [10]. Inorganic material such as tungsten oxide (WO_3) reported by Deb in 1969 is the pioneer class of ECDs [11]. Since then a great amount of studies and researches have conducted on these materials however, there are still problems associated with them mainly; slow switching time and high cost of vacuum evaporation. Small organic molecules are the alternatives which are utilized as chromic layer in device. Viologen (1,1'-di-methyl-4,4'-bipyridilium) has been studied extensively for years and commercialization has been done for rear view mirrors. Dication form of viologen is transparent but radical cation molecules which have intense deep blue color can be formed as a result of reductive electron transfer and by changing the alkyl groups on nitrogen, color change in radical cation redox state can be achieved e.g. 4-cyanophenyl instead of alky group transmits green [12].

Promising properties such as ease of processing, fast switching time and high efficiency in coloration in conjugated polymer based electrochromic devices have drawn great amount of attention [9]. These semiconductors change their color upon applied potential. In other word, electrochemical redox of polymer result in changing in absorbance of polymer. Upon oxidation of the polymers polaron which bears positive charge forms on back bone of the polymer. These positively charged moieties are concomitant by flux of counter ion from electrolyte. If this partially doped state be further oxidized bipolaron can be formed that facilitate the reduction of bandgap. Hence, during redox reaction band gap changes consequently the observed color. In fact, EC martials can be divided into three classes based on their optical states [13]. First type is distinguishable in the sense that it consists of one colored state and a transparent one like poly (3, 4-ethylenedioxythiophene) known as PEDOT which are used in applications related to smart windows [18,17]. The other type has discrete colored states and does not have a bleaching state. They are used in

display panels since different redox colors are required. To mention an example of this type thin film of polythiophene which could switch from blue to red would be an appropriate one. The last type are polymers with more than two colored states and get attention because of their versatility in EC applications like poly(3,4-propylenedioxyppyrole). Fundamentally there are five parameters which make these EC materials distinguishable. Firstly, the percent transmittance of an ECD at different wavelengths on electromagnetic spectrum can be inferred from optical contrast. More specifically the amount of light with a certain wavelength that is reflected. Furthermore, optical stability at different potentials and optical bands on spectrum can be investigated by considering the cycles showing transmittance change. Next, deterioration of the active layer accounts for stability which affects the efficiency of ECD. Irreversible redox reactions, heat dissipation and side products from electron loss or gain processes upon oxidation and reduction of the materials and contaminants are some of the most notable reasons that result in the deterioration. Thirdly, the time it takes for a color transformation in materials to be observed during oxidation and reduction processes which is known as switching time or switching speed in the literature. Surface characteristics of thin films, conduction of free charges in electrolyte and permeability of ions to the interface of the thin films are factors that affect the switching time. Another distinguished parameter associated with EC materials is related to how well an EC device functions i.e. coloration efficiency (CE). In order to calculate the CE value, Q_d charge transferred per unit area, charge in optical density (OD) need to be known. The equations 1 and 2 show these relations clearly [15].

$$\Delta OD(\lambda) = \log \frac{T_b(\lambda)}{T_c(\lambda)} \quad \text{Equation 1}$$

$$\frac{OD(\lambda)}{Q_d} = \frac{\log \frac{T_b(\lambda)}{T_c(\lambda)}}{Q_d} \quad \text{Equation 2}$$

where;

η (cm² /C): The efficiency of the CE

T_b : Transmittance value at the bleached state

T_c : Transmittance value at the colored state

1.2 Conjugated Polymers:

Over past 50 years macromolecular science has had major impact in human life style. From spandex in fashion to drug delivery systems polymers emerge not only alternative materials but also promising ones. Recent advances in polymer science and with new applications being researched, there is no reason to believe that the revolution will stop any time soon. New area in polymer science was introduced in 1970s by discovery of Hideki Shirakawa, Alan J. Heeger and Alan G. MacDiarmid. They show that polyacetylene becomes conductive as a metal. In 1974, Shirakawa and coworkers prepared polyacetylene utilizing Ziegler-Natta catalyst as a silvery film. In spite of its metallic appearance it was not conductive. However, by coworking of above mentioned scientists, oxidation of this polymer by halogen vapours made it 7 orders of magnitude conductive than the former form of polyacetylene [16]. In fact, treatment of polymer with halogens called ‘‘doping’’ like doping process in semiconductors. The presence of conjugated system on polymer backbone is the key property in conductive polymers. In this system each bond has one localized sigma (σ) bond which covalently hold atoms in molecules and double bond delocalize π system. In fact, presence of a conjugated system makes polymers conductive. The formation of charge carriers which are mainly electrons and holes is vital for conductivity. The electrons can tunnel from neighboring position and fill the hole result in formation of new hole. Hence, charge migration to long distance happens by this mechanism.

Redox processes abstract electron or add electron to polymer. For example, in case of polyacetylene iodine forms a triiodide ion. Removing of electron from valence band of polymer create a hole which is localized and stabilized by counter ion, in this case triiodide. This radical cation is known as polaron. By further oxidation of the polymer bipolaron can be formed [17]. Besides solitons which are free radicals can also be formed on backbone of the polymer by isomeration or bond length alternation

[18]. This neutral free radical can propagate in the polymer by transferring itself to a neighboring polymer by hopping. This process called intersoliton hopping **Figure 1** [19].

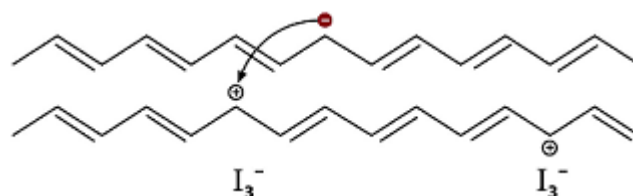


Figure 1. Schematic Presentation of intersoliton hopping.

After surprising discovery in 1970s, advance in in field have grown and semiconducting properties of polymer draw attention in both industry and academia. OPVs, OLEDs and OFETs are examples of such applications where conjugated polymers were investigated in world wide. The mechanism, device architecture and polymer characteristics are the main reasons that should be taken into account to promote efficiency. The optically doping process are different than electrochemical doping in these active compounds. The doping in these semiconductors is done by formation of exitions. Before a detailed introduction of OPVs and PLEDs, band gap which is an inherent property of semiconductors should be explained to clarify conductivity of these materials. In fact, it is defined as the energy difference between the highest occupied molecular orbital (HOMO) and the lowest unoccupied molecular orbital (LUMO) energy levels or in another words the energy between conduction band and valence bands of the materials [17]. Considering electrical conductivity, materials are classified as conductors, insulators and semiconductors. The valence band is partially filled in conductors that leaves empty space for electrons to move along when exposed to an electric field. In insulators all valence band is completely filled and conduction band is completely empty separated by a large energy band gap. However, in semiconductors it is just the opposite of insulators. Electrons can move to the conduction band from valence band. **Figure 3** represent the band energy structures of different materials. Cyclic voltammetry and photoemission yielding spectroscopy are used to determine the HOMO and LUMO

levels. The optical band gap can be determined from absorption onset of visible absorption of polymers.

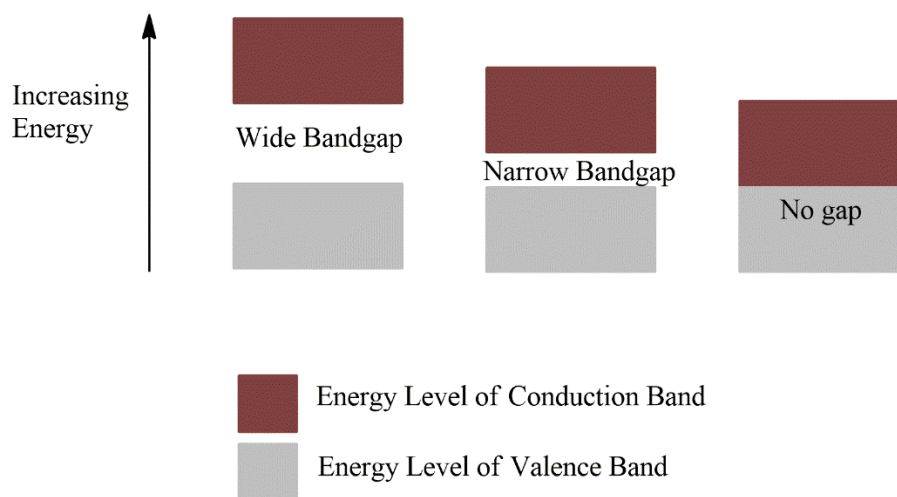


Figure 2. Band Gap Diagram.

1.2.1 Band Gap Engineering

By tuning the band gap (E_g) electronic properties of semiconducting polymers can be tailored and it is often called E_g engineering. Understanding the effect of structural factor will be helpful for designing optimum band gap. Conjugated polymers have two resonance forms that are nondegenerate. These are aromatic and quinoid structures. In the aromatic form π electrons are confined, whereas, in quinoid form of the polymer π electrons are delocalized along the conjugated polymer chain which simultaneously alter a single bond to a double bond and vice versa. These structures are depicted in Figure 3a. The aromatic form of the polymer is more stable energetically, however, the quinoid form has higher energy resulting in lowering the band gap. Due to strong dependency of E_g on alternating in conjugated system, five geometrical parameters will be discussed. The first one is bond length alternation denoted as BLA [20]. This can be defined as difference in bond lengths of multiple bond and adjacent single bond. When quinoid structure is dominant in ground state more double bond pops up between adjacent rings. Consequently, BLA decreases

and narrows the band gap. This factor can be quantified as E_{BLA} . Another factor is energy that require to transform aromatic structure to quinoid form. Hence, reducing the aromatic stabilization resonance will narrow the band gap. The effect of this parameter is quantified as E_{res} [21]. The third one is Substituents Effect, E_{Sub} , which is the most utilized way in adjusting HOMO and LUMO. Introducing electron donating group usually increases HOMO level and inserting electron withdrawing group to polymer increases ionization potential and electron affinity. Last one is a rotational disorder around the single bond E_{θ} [22]. This angle known as dihedral angle which increases E_g as angle increases. By considering these factors E_g can be expressed with the following formula. The effect of all above mentioned factors are represented in **Figure 3b** [23].

$$E_g = E_{BLA} + E_{res} + E_{Sub} + E_{\theta} \quad \text{Equation 3}$$

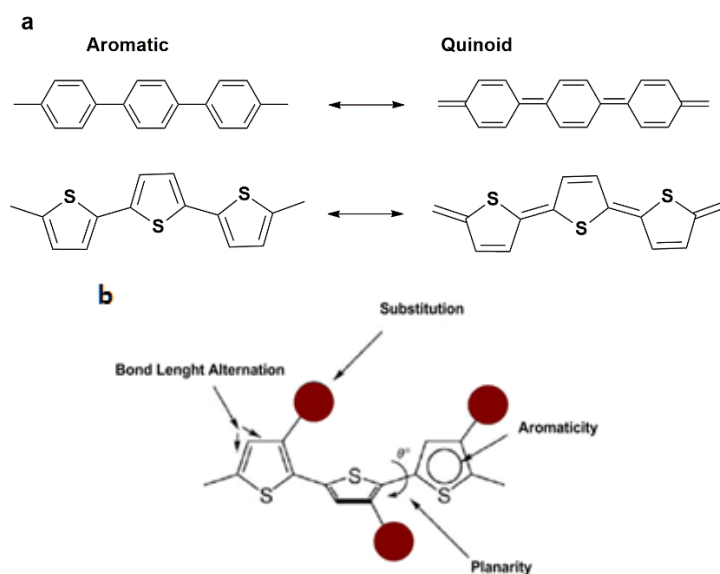


Figure 3. a) Resonance Structure of Polymers. b) Factor Effecting Band gap

1.3 Organic Photovoltaics

The PV effect can be described as direct conversation of light to the current. Utilizing organic based materials as the active part for PV devices is called OPVs. In

OPVs, small molecules or polymers can be used as the absorbing layer for the generation of current. However, the potential of inkjet printing, recent advances in synthesis of material beside engineering bandgap make conjugated polymers as the promising materials for OPVs. In these devices electron rich polymers behave like electron donor which is blended with electron acceptor materials such as phenyl-C₆₁-butyric acid methyl ester (PCBM). As a requirement these polymers should have a conjugated π system. An example of extensively studied conjugated polymer; poly-3-hexyl thiophene (P3HT), and electron accepting PCBM are presented in **Figure 4**.

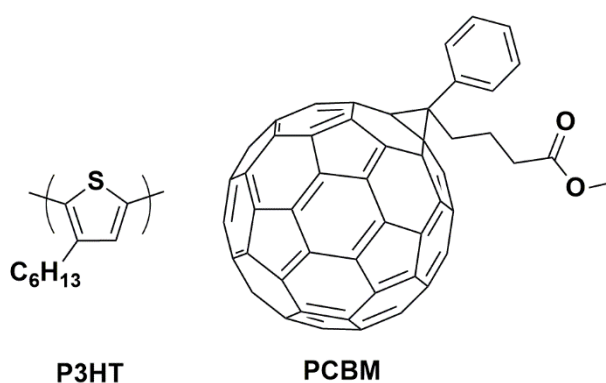


Figure 4. Conjugated Polymer P3HT as the Donor and PCBM as the Acceptor.

In addition to design and developing materials, optimization of interface and developing device structure will be helpful for commercialization. By placing these factors in forefront the efficiencies of these devices have been boosted from 2.4% to 11.7% in the last decade [5]. For example, recently Yuan and et al demonstrated that by utilizing novel additive and hydrocarbon solvent, morphology can be controlled which leads to boosting of PCE from 6.7% to 11.7%. The chemical structure of this polymer is depicted in **Figure 5**.

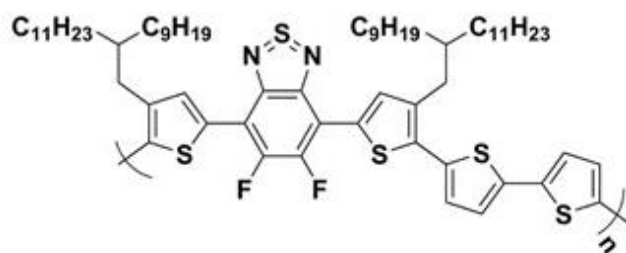


Figure 5. The Structure of the Polymer That Shows Highest PCE Performed Polymer in Literature.

The working principle of organic PVs is depicted in **Figure 6**. These steps are; **1.** Photo induced exciton formation, **2.** Diffusion of excitons, **3.** Charge separation and **4.** Charge transport. The properties of each layer will be discussed later in this section.

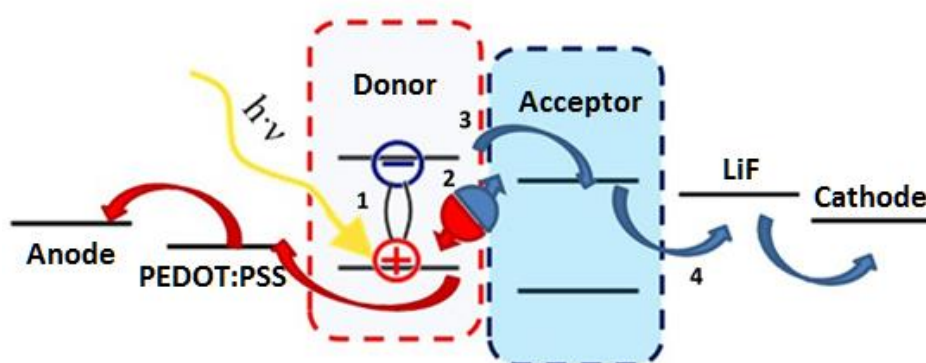


Figure 6. Working principle of an OPV.

1. Photo induced exciton formation: The photon absorption of conjugated polymer and efficiency of OPVs are directly related to each other. As light is absorbed, excitation; an electron-hole pair forms. The formed excitations are called Frenkel excitons. This form of excitations are localized on backbone of polymer hence extra energy is required to overcome excitation binding energy and generate free charge carriers. Typically binding energy in organic material's between from 0.3 and 1 eV[24].

2. Diffusion of excitons : Excitons have very short life times and during their lifespan they cover a certain distance called as excitation diffusion length. The diffusion of excitation can be describe with two mechanisms regarding their electronic states. Singlet electronic state excitations diffuse via Förster Resonant Energy Transfer (FRET) [25]. Dipole-dipole coupling interaction between donor and acceptor describes this long range energy transfer (1-10 nm). Whereas, Dexter energy transfer in which overlap of wave functions are required, triplet-triplet and singlet-singlet energy transfer is allowed. These two mechanisms are depicted in **Figure 7**. This is worth to say that former mechanism is valid to describe hopping mechanism in polymer backbone whereas the intermolecular intersoliton hopping mechanism usually is described by hopping into empty states by randomly distributed Density of States [26]. The diffusion via these mechanisms to reach interface of donor-acceptor is crucial for current generation. Hence, larger diffusion length enhances current generation. However, as diffusion length increases another factor should be considered which is exciton life time. In fact, via reducing in film thickness, both these factors could be fulfilled. However, thinner film diminishes photon absorption which is a drawback for current formation. Therefore, exciton lifetime, diffusion length and film thickness should be taken into consideration to engineer high performance OPVs.

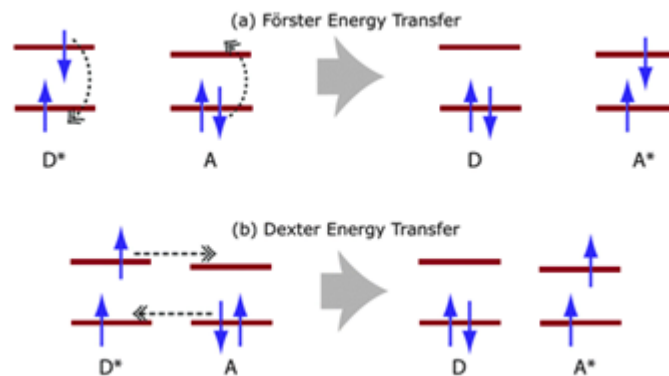


Figure 7. Foster and Dexter Energy Transfer.

3. Charge separation: After diffusion of exciton to interface electron from LUMO of the donor transferred to LUMO of the acceptor. The driving force for this transition is energy difference of these two levels. After transferring process, the electron in LUMO of the acceptor and hole in HOMO in donor interact by Columbic forces. In CT states electronic structure of this state and morphology plays a crucial role.

4. Charge transport: One of the vital factor to increase efficiency of OPVs is understanding of charge carrier transport and collection. The imbalance mobility of charge carriers results in formation space charge (or depletion region) build-up which dramatically decreases efficiency of the device. In bulk heterojunction devices electron mobility usually is 2-3 orders of magnitude higher than hole mobility [27]. Because of difference in mobility of hole and electron, the possibility of recombination increases [28]. In order to overcome this issue, thermal treatment have been done. For example, Valentin et al show that the hole mobility of P3HT increased 3 orders of magnitude by thermal annealing [27]. In fact, optimized thermal annealing controls orientation and crystallization of polymer which improve CT and collection at corresponding electrodes.

1.3.1 Toward High Performance OPVs:

In order to develop high performance OPV cells certain principles are needed to be taken into consideration. E_g can be optimized by considering donor acceptor approach.. Performance of the device can be further improved by bulk heterojunction architecture where a greater interface area between polymer and acceptor is obtained. Increasing the performance of the cell for the purpose of harvesting the solar energy requires high absorption by polymer. Hence, it is expected that PCE can be higher for a polymer having narrower E_g that absorbs in Near-Infrared region. The performance of cell is affected by morphology of polymer and acceptor where to have a high interface area is demanded. It is note-worthy also to mention that efficiency is reduced by trapped domains where polymer and acceptor have not or little interface with electrodes.

1.3.1.1 Donor Acceptor Approach

Hoeve and coworkers were the first who offered Donor-Acceptor (D-A) approach for the first time in 1963 (see **Figure 8a**). Tuning the HOMO and LUMO energy levels and thus E_g can be accomplished using this modality for conjugated molecules. There are two moieties associated with this approach; donor and acceptor molecules. One, the donor moiety which is electron rich and the acceptor has an electron deficient nature. Via hybridization of these moieties, a new HOMO level mainly located at donor moiety and a LUMO level located at acceptor moiety form [33,27]. New HOMO and LUMO levels that arise from this hybridization are shown in **Figure 8b**. Some examples of electron donor and acceptor moieties are shown in **Figure 8c**.

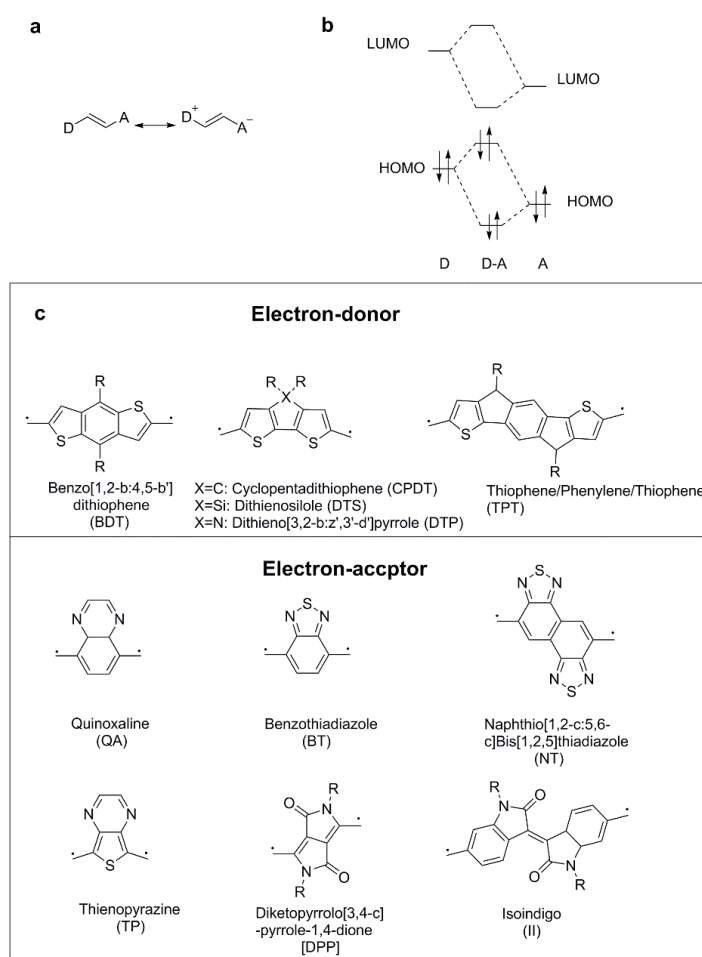


Figure 8. a) Donor and Acceptor Approach b) Hybridization resulting from D-A approach c) Donor or Acceptor Moieties reproduced from[23].

1.3.1.2 Narrow Band Gap:

Most efficient OPVs harvest much of the near-IR and visible regions of solar radiation. As seen in **Figure 10** these are the regions of maximum solar flux, therefore there has been a great deal of attention focused on creating organic donor and acceptor layers with lower band gaps (1.2 to 1.6 eV), without sacrificing of chemical stability [32].

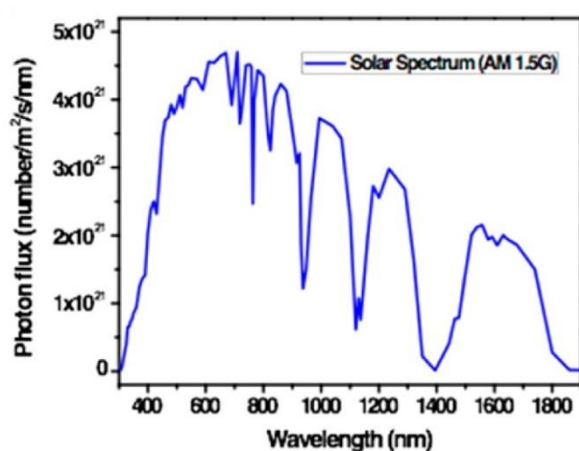


Figure 9. Solar Spectrum in 1.5 G Condition Reproduced From [33].

1.3.1.3 Morphology Optimization:

Since the mixed thin film is not an equilibrium structure, phase segregation of this mixture into an entangled heterojunction can be obtained by annealing the films at optimal temperatures which will crystalize the film internally into the bulk structure. However, a reduction in efficiency can be observed in some cases. This result shows that the phase separation has resistive cul-de-sacs where the free charge has been trapped before their collection at the electrodes [34].

1.3.2 Characterization of OPVs

In order to determine characteristics of PV cells, the J - V relation is investigated in Air Mass (AM) 1.5 global condition. From this curve important parameters are determined; J_{sc} and V_{oc} . Hence, knowing the relation of current density and potential, Fill Factor (FF) and PCE can be determined.

1.3.2.1 Short Circuit Current Density

The current which is generated when there is no external potential is called J_{sc} . It has direct relation with external quantum efficiency (EQE) which is the ratio of the number of incident photons to the number of generated charge carriers. This relation is formulated in equation 4.

$$EQE = \eta_A * \eta_{ED} * \eta_{DA} * \eta_{CT} * \eta_{cc} \quad \text{Equation 4}$$

η_A is a parameter which is correlated with the light absorption efficiency. As the band gap decreases the capability of light absorption increases, hence, EQE increases. η_{ED} is the ability of exciton transfer of the interface of polymer and acceptor. The main parameters affecting the diffusion performance is the morphology of the active layer. Dissociation efficiency of excitons is known as η_{da} . The donor-acceptor interface creates a charge transfer state. In this state the electron and hole are not separated. Increasing the driving force for dissociation of the exciton at interface increases this parameter. This force should be more than the exciton binding energy which is about 0.3 eV. η_{CT} is the charge transfer to the corresponding electrode. The migration of charges in the active layer is explained via hopping process influenced by defects on the active layer and recombination of the excitons. η_{cc} is the efficiency which explains the ability of electrodes for charge collection. Taking such consideration on electrodes will increase charge flow and diminish formation of space charge region on electrode and consequently current density[28,39].

1.3.2.2 Open Circuit Voltage

The potential measured between two electrodes when the current value is zero is

called V_{oc} . This phenomenon can be described with tangible data with some empirical approximations. V_{oc} value of the device is described as the energy difference between HOMO of the donor and LUMO of the acceptor molecules. By the Scharber's studies on this issue, a formula identifying the experimental V_{oc} value was published in 2006[36].

$$V_{oc} = \frac{1}{q} (E_{HOMO(D)} - E_{LUMO(A)}) - 0.3 \text{ V} \quad \text{Equation 5}$$

The V_{oc} loss of 0.3 eV is empirical, and the loss could be greater or smaller. It is known that introduction of electron donating or withdrawing group on polymer backbone result in tuning the relative energies of HOMO and LUMO [41,42]. Electron donating group increase the HOMO level and electron withdrawing one diminish LUMO level. Therefore, tailoring the HOMO and LUMO levels V_{oc} can be tuned.

The recombination of carriers at donor acceptor interface develops dark saturation current, resulting in the reduction of V_{oc} in open circuit condition which can be expressed by equation 6 [39].

$$V_{oc} = \frac{mk_bT}{q} \ln\left(\frac{J_{ph}}{J_0} + 1\right) \quad \text{Equation 6}$$

To inhibit the recombination, in other words, increase V_{oc} , they are several considerations to be taken into account. The dissociation of excitation strongly depends on electric field at interface of donor-acceptor, hence, as the built in electric field is larger, excitation dissociation gets easier and a higher V_{oc} is expected. Tada et al showed by changing dipole moments of P3HT or PCBM can tune V_{oc} from 0.3 to 0.9 V. In another approach Yuan and colleagues incorporate a ferroelectric polymer layer in structure of device to increase internal electric field which enhanced efficiency from 1-2% to 4-5%. In addition, hole/electron blocking layer effectively reduces recombination at the surface of the corresponding electrode which suppresses dark current. In fact, many hole blocking materials are reported on deep

laying HOMO which also increase V_{oc} [29].

1.3.2.3 Equivalent Circuit

Although the working principle of the OPVs are not based on p-n junction, the equivalent circuit is applied for these semiconductors [39]. Circuit for J-V characteristics OPVs can be described by Shockley's theory which consists of a diode, constant current source and an external load. However, this is the case for an ideal device, Hence, the current losses across the circuit should be considered. These losses are modeled as shunt resistance (R_{sh}) and series resistance (R_s). R_{sh} originates from current leakage from edge of the cell or extrinsic impurities, whereas, R_s comes from resistance of electrode and polymer. The equivalent circuit depicted in **Figure 11**.

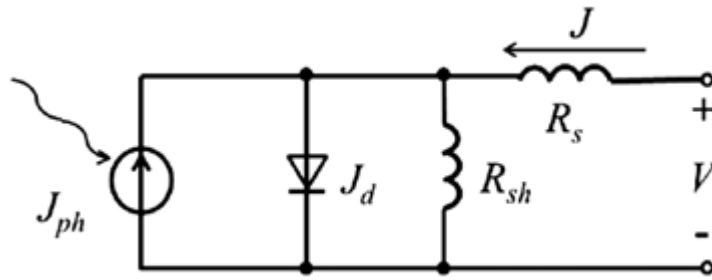


Figure 10. Equivalent Circuit of Organic Semiconductors Reproduced From [39].

By considering the Shockley's theory and these resistances, the recorded current density on load can be formulated as:

$$J(v) = \frac{R_{sh}}{R_s + R_{sh}} \left\{ J_0 \left(e^{\frac{q(V - JR_s)}{nK_b T}} - 1 \right) + \frac{V}{R_{sh}} \right\} - J_{ph} \quad \text{Equation 7}$$

Here J_{ph} represent photoinduced current density, V is the applied potential, k_b is boltzmann constant, T is temperature, n is ideally factor, q is charge, J_0 represents reverse saturation current density and J is current density in external load [40].

1.3.2.4 Fill Factor and Power Conversion Efficiency

Fill Factor (FF) determines how easy or difficult to extract charge carriers out of the device. In fact, it shows the relation between the recombination and transportation of the charge carriers. The recombination of carriers and FF are inversely proportional to each other, as FF raises recombination diminishes. FF strongly depends on the quality of diode. The deviation from ideality in FF can explain by shunt and series resistances. For ideal case R_s is zero and R_{sh} should be infinity. The FF can be easily calculated from J_{sc} and V_{oc} by equation 8 [41].

$$FF = \frac{J_m V_m}{J_{sc} V_{oc}} \quad \text{Equation 8}$$

Where J_m and V_m correspond to current density and voltage at maximum power output. **Figure 12** shows the maximum power of the cell and ideal cell which represented as A_1 and A_2 respectively. PCE is ratio of the produced electricity to incoming light. In fact, PCE is work done by PV cell and can be formulated as equation 9[41][23].

$$PCE = \frac{J_m V_m}{P_{in}} \quad \text{Equation 9}$$

Where P_{in} is input or power of incoming light.

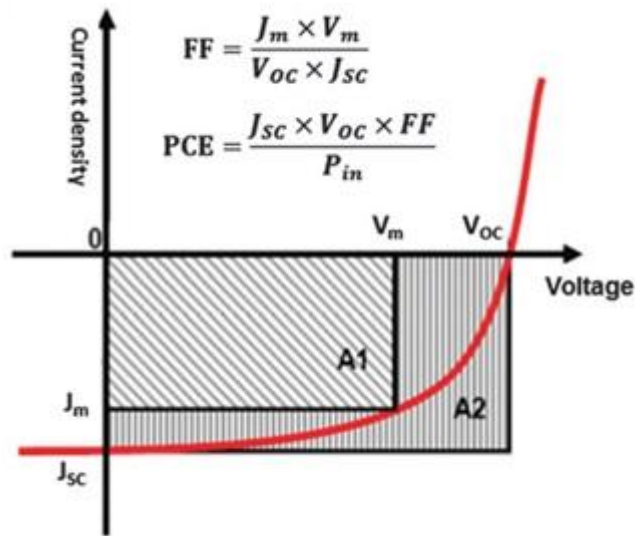


Figure 11. The Fill Factor and an Ideal cell Fill Factor reproduced from [23].

1.4 Organic Light Emitting Diode

Availability of tailor-made functional organic materials that can be used as well-controlled thin films is the main reason for development of OLEDs. Thereby the requirements to the materials are manifold: starting from processibility and film formation via electrical transport to optical properties. Polymeric substances and small molecule materials are the two classes of commonly used organic light-emitting devices. Possibility to use simple screen printing i.e. wet deposition techniques which allow fabrication of large area devices is yet another advantageous aspect of polymer based optoelectronics. Since electroluminescence is responsible for lightning in LEDs, it is worth to have a closer look at this phenomenon. Radiative recombination of electrons and holes is inflicted by an external electrical field resulting in electroluminescence. In PLED, charge carriers are injected via a voltage source of few volts through electrodes i.e. holes from anode and electrons from cathode. Electron-hole pair is formed in the active layer when electrons and holes first meet which result in a radiatively decaying photon emission. The working principle of OLEDs or PLEDs can be described in 4 major steps. These are shown in

Figure 13. The process begins by injection of electron from aluminum electrode and hole from ITO. Charge carriers transferred through organic layer which is the active part of device. In organic layer bounded electron hole pairs, in other words, excitons are formed and finally these excitons decay and light is emitted[42]. The single layer device can be constructed by spin coating the HTL on ITO supported glass. Lithium fluoride about 1nm is physically evaporated then aluminum is evaporated in same way by rate of 0.4 Å per second. The structure of the device is depicted in **Figure 14.**

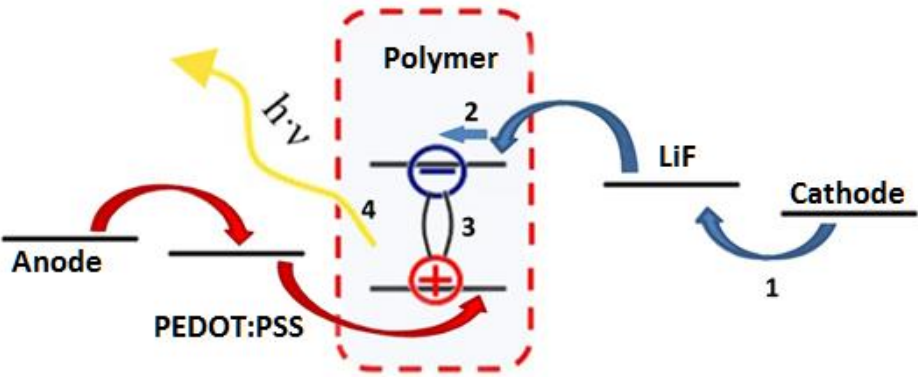


Figure 12. Working Principle of OLED

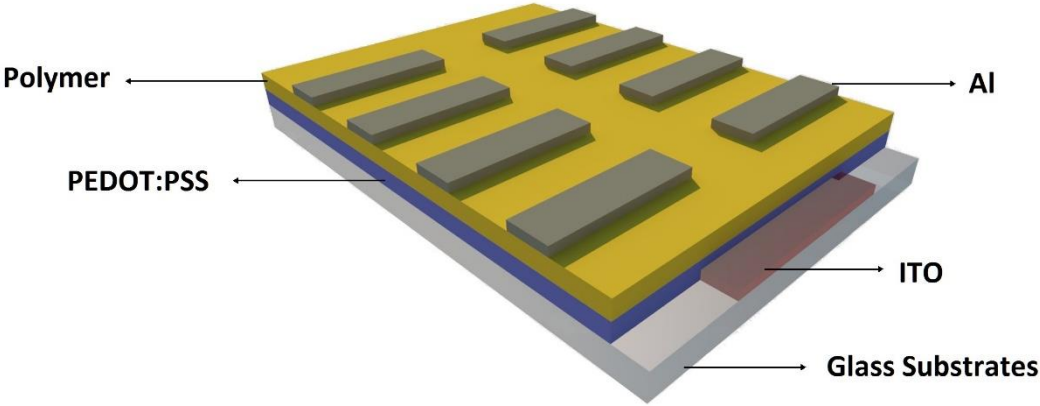


Figure 13. Single Layer OLED Device structure

Energy is radiated via fluorescence or phosphorescence in electrically excited molecules. Their mechanism is depicted in **Figure 15**. Based on spin statistics of quantum mechanics singlet and triplet states are classification of electrically excited excitons in organic molecules which show an electronic state density ratio of 1 to 3 respectively[47,48]. One notable difference between fluorescent molecule and phosphorescent one is that usually phosphorescent is not emissive due to long life time (about 10^{-6} s). Hence, this limits Internal Quantum Efficiency (IQE) to maximum 25%. One of approaches to increase internal QE is utilizing a heavy metal atom such as iridium or platinum. Introduction and development of emitters based on heavy-metal centered organic complexes was considered as breakthrough in the advancements on subject. In these compounds, phosphorescence becomes an allowed transition since strong spin-orbit coupling mixes triplet and singlet CT states. In spite of high efficiency of these materials, limited availability and stability of deep blue phosphorescent emitters remain as an issue [42].

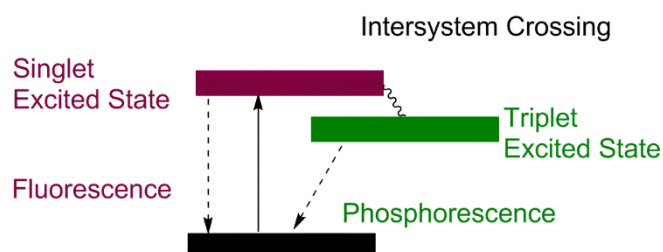


Figure 14. Fluorescence and Phosphorescence radiative decay.

1.4.1 White Organic Light Emitting Diodes:

One of the advantage of organic emitters is their broad luminescence spectrum [45]. Generation of light spreading over the whole visible spectral range is possible when several organic emitters with different emission color are combined. In order to achieve efficient white light emission in single layer devices three primary colors or two complementary colors are utilized in active layer. To achieve this,

monochromatic emitters are physically blended or light emitting moiety are introduced in polymers, back bone. However, because of delicacy in control of charge recombination and energy transfer processes between the different polymers, it was not very easy to achieve white light emission with good and stable color quality. Nowadays it is more common to employ distinct emissive layer for RGB that can either be directly stacked on top of each other which is called multi-layer device. Hence, it is possible to cover a large variety of colors and color temperatures depending on the method and the choice of materials. However, formation exciplex have reported by many groups at interface of the layer which results in broad emission of light. This could be a drawback for monochromatic light emission whereas for white light utilizing this emission to compensate blue emission is possible [50,46].

1.4.2 Color Quality of Polymer Light-Emitting Devices

The color quality of the OLEDs and PLEDs is assessed by colorimetric quantities. These quantities are color temperature, chromaticity and color rendering indices (CRI). The comparison between chromaticity of light source with blackbody radiator determines color temperature. More precisely, it is the temperature is needed to heat blackbody radiator to emit light which is equivalent to the color of light source. For example, for blackbody to radiate green-blue color which is known as cold color 5000 K or above is required, whereas, for red yellow (warm colors) 2700-3000 K is enough. Color rendering indices define as capability of the source to reproduce the colors of objects in comparison with daylight. It is a quantity between 1 and 100 where revealing the color in range of 70-100 has excellent CRI. The chromaticity of the light source can be coordinated by Commission Internationale de l'éclairage (CIE) diagram. In fact, this diagram used to define the purity of the color source in visible region[46].

1.4.3 Characterization of Polymer Light-Emitting Devices

There are three main factors to characterize efficiency of OLEDs and PLEDs. These parameters are quantum efficiency (QE), luminous efficiency (LE) and power efficiency (PE).

The LE is the ratio of luminance to the given current density where luminance is intensity of light at particular direction. In other word, luminance can be defined as the response of human eye to light. The luminance strongly depends on the wavelength. Hence, human eye best responds to green color (555 nm) which have highest value of luminance at a specific power. QE can be divided into EQE and IQE. EQE is the number of photon emitted per number of injected charge carriers. Whereas, IQE is radiative recombination of excitons to the total recombination (nonradiative and radiative). PE is ratio of luminous intensity to the input power where luminous intensity is the power emitted by a source in specific direction. It can be obtained by equation 10.

$$PE = \pi \frac{LE}{V} \quad \text{Equation 10}$$

Where V stands for applied potential and LI is luminous intensity. The luminous flux (LE in lumen) and luminous intensity (candela) can be correlated in PLEDs as 1 candela = π lumen [46].

1.5 Motivation of Study

Derivatives of phenanthroimidazole are known to be efficient for hole blocking or electron injection as well as superb thermal stability. The X-ray single crystal studies of phenanthroimidazole derivative clearly reveals the effect of dihedral angles of phenanthroimidazole. In this study, the imidazole ring and thiophene ring are almost coplanar which enhances conjugation as depicted in **Figure 16a**. In addition, thiophene and imidazole rings of neighboring molecule are arranged face to face which result in efficient π - π stacking as seen in **Figure 16b**. However, the presence

of pendulum on nitrogen atom of imidazole ring harks π - π stacking of benzene ring, hence it prevents self-quenching [47]. Cheng et al showed that polymerization of phenanthroimidazole derivative of thiophene moiety with thiophene as donor are not amply coplanar because of created steric hindrance. But, they demonstrated that incorporation of this moiety on poly(3-hexylthiophene) results in fast CT by excited state deactivation and lower the E_g of this polymer which leads to improvement of J_{sc} from 8.7 mAcm^{-2} to 14.2 mAcm^{-2} . Hence, the PCE enhanced to 2.8% for copolymer from 1.22% for pure of poly(3-hexylthiophene). These properties suggest phenanthroimidazole as a promising candidate for both OLED and OPV applications [48].

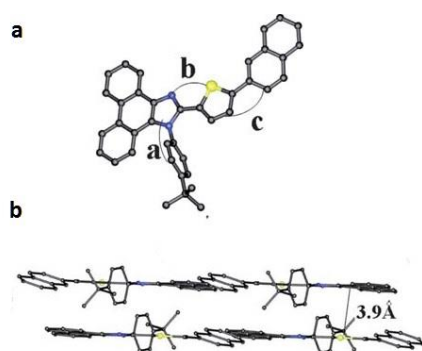
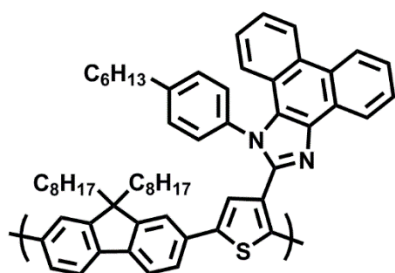


Figure 15. Corresponding Angle of Phenanthroimidazole derivative of thiophene reproduced from [47]

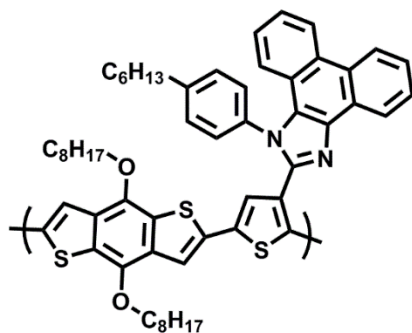
In literature the commonly used donor compounds can be divided into three categories which are weak, medium and strong relative to each other. The two donors that have been used in this study belong to weak and medium donors regarding their applications [29]. The fluorene is regarded as the two fused benzene ring bridged by carbon which fixes the tricyclic system and makes them coplanar. The relatively electron deficient nature of this compound and relatively high E_g than the other categories placed it as the weak donating material. However, fluorene have relatively high quantum yield for OLED application and excellent soluble-processing. In

addition, copolymerization with small band gap monomers creates randomly dispersed low energy traps that increases the probability of recombination as regards to the type of application. On the other hand, benzodithiophene (BDT) derivatives are regarded as medium donor because of their electron rich structure. BDT have specific characteristic due to coplanar and rigid structure as well as symmetric configuration, in fact, BDT derivatives have strong intermolecular π - π stacking which is crucial for efficient CT. By considering the absorption spectrum and above mentioned characteristics the fluorene based polymers are used for OLED and BDT based polymer, are utilized as active layers for PV applications.

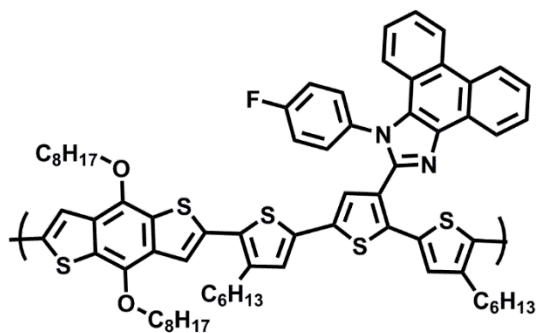
In this study, three new polymers were synthesized and their optoelectronic properties were studied. By considering the donor-acceptor approach phenanthroimidazole based moieties was considered as the acceptor. There are strategies in designing these polymers that worth to indicate. For example, alternating BDT and electron withdrawing phenanthrene-imidazole group expected to improve electron transfer of BDT. Beside this, it is expected introduction of this electron deficient unit increase effective conjugation path, hence reduction in band gap. In addition to this, in **P3**, 3-hexylthiophene bridge was incorporated in backbone of polymers in order to increases the planarity of monomer. This bridge not only increase the solubility of corresponding monomers but also results in diminishing bad gap of the polymers due to enhancing conjugation path. Also incorporation of fluorine atom in benzene ring expected to reduce electron density on benzene ring, hence the acceptor would be more electron deficient. This **Figure 17** shows the polymer structures that have been studied in this work.



P1



P2



P3

Figure 16. Structure of the Polymers.

CHAPTER 2

EXPERIMENTAL

2.1 Materials

The chemical reagents utilized in syntheses were supplied from Sigma-Aldrich and Alfa Aesar and used as received. All solvents that used in reactions were freshly distilled in the presence of benzophenone and metallic sodium. Merck Silica Gel with 60 mesh was used for column chromatography as the stationary phase. The synthesized chemicals were characterized by ^1H and ^{13}C Nuclear Magnetic Resonance Spectroscopy (NMR) on Bruker Spectrospin Avance DPX-400 Spectrometer. The deuterated chloroform was used as the solvents in NMR analysis and tetramethylsilane was the reference. All reactions were monitored by thin layer chromatography (TLC) supplied by Merck and the products was synthesized according to literature.

2.2 Instrumentation

2.2.1 Electrochemical Studies

In order to investigate the semiconducting properties of the polymers electrochemical studies were performed via Voltalab 50 potentiostat. In this system ITO, platinum and silver were working, counter and reference electrodes respectively. The solvent was acetonitrile and the electrolyte was 0.1 M tetrabutylammonium hexafluorophosphate (NBu_4PF_6) for **P3**. For **P1** and **P2** same solvent was used whereas lithium perchlorate and sodium perchlorate (1:1 mole ratio) was used as electrolyte. The reduction and oxidation (redox) behaviors of polymers were

investigated by cyclic voltammetry (CV). The electronic band gap of the polymers was determined by measuring HOMO and LUMO. Potential of normal hydrogen electrode to vacuum level was the reference (-4.75 V). Hence, LUMO and HOMO were determined by $\text{HOMO} = -(4.75 + E_{\text{onset}}^{\text{ox}})$ and $\text{LUMO} = -(4.75 + E_{\text{onset}}^{\text{red}})$.

2.2.2 Spectroelectrochemical Studies

Spectroelectrochemical studies were conducted by Varian Cary 5000 UV– Vis spectrophotometer to measure absorbances of neutral, polaron and bipolaron states. The polymers were coated on ITO by spray coating method. The films were oxidized by step wise applying potential. The first absorption peaks correspond to π - π^* transitions of neutral film. The onset of maximum absorption was determined by taking tangent line of the neutral film. Using the maximum absorption onset, the optical was determined by converting the wavelength to electron volts. After oxidation of films by applying step wise potential the polaron and bipolaron band emerged. The maximum absorption of these band was determined by UV-Vis-NIR spectroscopy.

2.2.3 Kinetic Studies

In order to investigate the percent transmittance changes between the maximum absorption of neutral and fully oxidized form of polymer in defined time interval kinetic studies was performed. To determine the maximum absorption UV-Vis-NIR spectroscopy was utilized. Beside this chronoamperometry was utilized to determine switching time of the polymer films.

2.2.4 Thermal Analysis

The thermal properties of polymers were investigated by Differential Scanning Calorimetry (DSC) and Thermogravimetric Analysis (TGA). The degradation of polymers was investigated by TGA of Perkin Elmer Pyris 1 with rate of 10 °C/min up to 700 °C under nitrogen atmosphere. The melting point (T_m) and glass transition temperature (T_g) of the polymers was identified by Perkin Elmer DSC Diamond with rate of 10 °C/min up to 300 °C under nitrogen atmosphere.

2.2.5 Gel Permeation Chromatography

The number and weight average molecular weight of the polymers was determined by gel permeation chromatography (GPC). The chloroform solution of polymers (4 mg/mL) was prepared and injected to the device. The lower molecular weight polymer would be interacting with stationary phase, hence retarded in column. According to the size distribution and polystyrene standard the molecular weight of polymers were determined.

2.3 Synthesis of 2,5-dibromothiophene-3-carbaldehyde

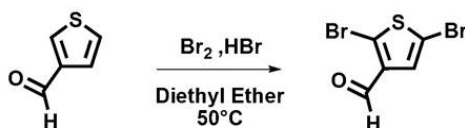


Figure 17. Synthesis of 2,5-dibromothiophene-3-carbaldehyde

A mixture of HBr (10 mL) and bromine (6.57 g, 2.15 mL, 41.1 mM) was added to mixture of thiophene-3-carbaldehyde (1.92 g, 17.10mmol, 1.50 mL) and diethyl ether (15 mL) in ice cold condition. After completion of addition, the mixture was heated to 50°C for 14 hours. The mixture was cooled to room temperature and quenched with saturated sodium bisulfate solution. The aqueous mixture was extracted with 40 mL diethyl ether 2 times. The organic layer was dried over sodium sulfate and solvent was removed under reduce pressure. The crude product was purified by means of column chromatography (hexane as the eluent) to give a pale yellow solid (3.51g ,77%). ^1H NMR (400 MHz, CDCl_3) δ 9.73 (s, 1H), 7.27 (s, 1H).

2.8 Synthesis of 2-(2,5-dibromothiophen-3-yl)-1-(4-hexylphenyl)-1H-phenanthro[9,10-d]imidazole

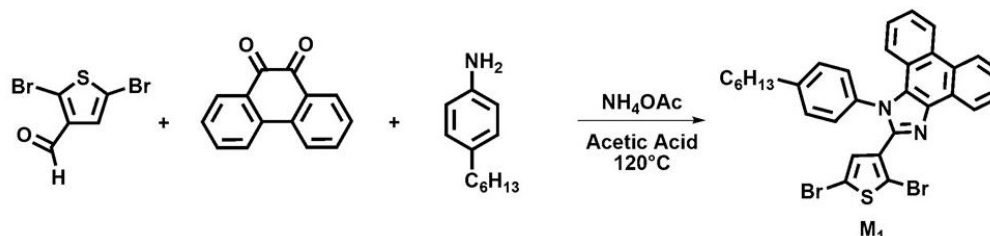


Figure 18. Synthesis of 2-(2,5-dibromothiophen-3-yl)-1-(4-hexylphenyl)-1H-phenanthro[9,10-d]imidazole

A mixture of 4-hexylaniline (1.64 g, 9.26 mmol, 1.80 mL), ammonium acetate (570 mg, 7.41 mmol), phenanthrene-9,10-dione, (390 mg, 1.85 mmol) 2,5-dibromothiophene-3-carbaldehyde, (500 mg, 1.85mmol) was charged in two neck round-bottom flask. The flask was purged by argon for 30 min. Then acetic acid (20 mL) was added and argon was bubbled for additional 30 min. The mixture was refluxed at 120°C for 12 hours. After completion of reaction, the solution was partitioned by 500 mL water and 50 mL chloroform. The organic layer was washed with brine. The organic layer was dried over sodium sulfate and concentrated under reduce pressure. The crude product was purified via column chromatography (1:1 hexane: dichloromethane) to obtain wheat color powder. For further purification the powder was washed with cold methanol (60mL) to give cream color crystals (630mg, 55%) named as M2. ^1H NMR (400 MHz, CDCl_3) δ 8.74 (dd, $J = 7.9, 1.1$ Hz, 1H), 8.67 (d, $J = 8.4$ Hz, 1H), 8.60 (d, $J = 8.2$ Hz, 1H), 7.65 (dd, $J = 11.0, 4.0$ Hz, 1H), 7.56 (ddd, $J = 8.3, 7.2, 1.4$ Hz, 1H), 7.46 – 7.40 (m, 1H), 7.25 (s, 4H), 7.19 (d, $J = 4.2$ Hz, 2H), 6.63 (s, 1H), 2.70 – 2.64 (m, 2H), 1.64 (dd, $J = 12.8, 5.8$ Hz, 3H), 1.27 (s, 8H), 0.84 (t, $J = 6.5$ Hz, 4H). ^{13}C NMR (101 MHz, CDCl_3) δ 143.90, 143.37, 136.27, 133.84, 131.32, 130.47, 128.81, 128.34, 127.76, 127.25, 127.03, 126.42, 126.11, 125.26, 124.69, 124.18, 123.03, 122.07, 121.73, 119.99, 118.91, 113.66, 110.10, 34.57, 30.63, 29.98, 27.77, 21.60, 13.09.

2.9 Synthesis of 2-(2,5-dibromothiophen-3-yl)-1-(4-fluorophenyl)-1H-phenanthro[9,10-d]imidazole

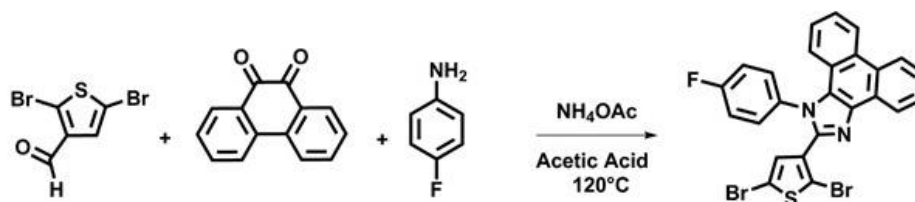


Figure 19. Synthesis of 2-(2,5-dibromothiophen-3-yl)-1-(4-fluorophenyl)-1H-phenanthro[9,10-d]imidazole

A mixture of 4-fluoroaniline (1.00 g, 0.88 mL), ammonium acetate (580 mg, 7.50 mmol) phenanthrene-9,10-dione (390 mg, 1.85 mmol), 2,5-dibromothiophene-3-carbaldehyde (500.00 mg, 1.85 mmol) was charged in two neck round-bottom flask. The flask was purged by argon for 30 min. Then acetic acid (20 mL) was added and argon was bubbled for additional 30 min. The mixture was refluxed at 123 °C for 15 hours. After completion of reaction, the solution was partitioned by 500 mL water and 50 mL chloroform. The organic layer was washed with brine. The organic layer was dried over sodium sulfate and concentrated under reduce pressure. The grey crude product was crystallized in hexane: dichloromethane (1:1) to give a white powder (560 mg, 56%). ¹H NMR (400 MHz, CDCl₃) δ 8.72 (d, J = 7.8 Hz, 1H), 8.66 (d, J = 8.3 Hz, 1H), 8.59 (d, J = 8.2 Hz, 1H), 7.68 – 7.61 (m, 1H), 7.56 (dd, J = 11.2, 4.1 Hz, 1H), 7.44 (t, J = 7.6 Hz, 1H), 7.37 – 7.30 (m, 2H), 7.26 – 7.20 (m, 1H), 7.17 – 7.08 (m, 3H), 6.69 (s, 1H). ¹³C NMR (101 MHz, CDCl₃) δ 162.99, 160.50, 143.17, 136.19, 132.20, 130.98, 130.27, 128.96, 128.23, 127.09, 126.26, 125.77, 125.21, 124.67, 124.18, 122.99, 121.89, 121.51, 121.32, 119.50, 115.79, 113.69, 110.45.

2.10 Synthesis of tributyl(4-hexylthiophen-2-yl)stannane

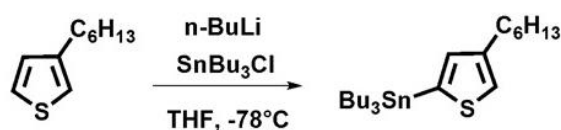


Figure 20. Synthesis of tributyl(4-hexylthiophen-2-yl)stannane

3-Hexylthiophene (1.00 g, 3.07 mmol) was dissolved in 20 mL anhydrous THF under argon atmosphere. The solution was cooled to -78°C. After 30 min, n-butyl lithium (1.5 mL, 2.5 M, 3.70 mmol) was added slowly to the solution in one hour. The mixture was stirred at this temperature for additional one hour. Then tributyltin chloride (0.52 mL, 3.69 mmol) was added to solution in 30 min. After 1 hour, the mixture was brought to room temperature and stirred for 12 hours. The solvent was removed under reduced pressure. The yellow oil was extracted by 50 mL chloroform and 100 mL water. Organic layer dried over sodium sulfate and concentrated under reduced pressure. The yellow oil (1.23g, 87%) was used without purification.

2.11 Synthesis of 2-(4,4''-dihexyl-[2,2':5',2''-terthiophen]-3'-yl)-1-(4-fluorophenyl)-1H-phenanthro[9,10-d]imidazole

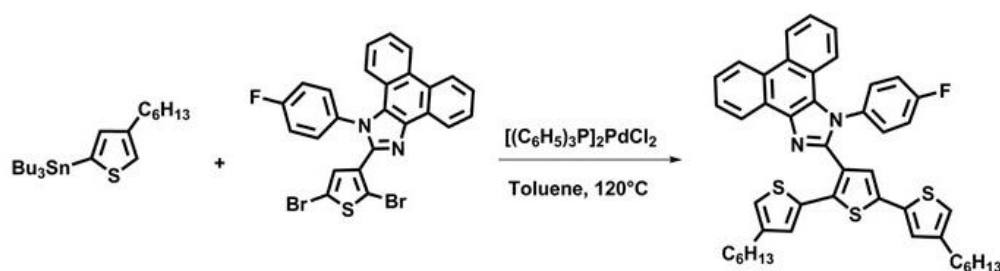


Figure 21. Synthesis of 2-(4,4''-dihexyl-[2,2':5',2''-terthiophen]-3'-yl)-1-(4-fluorophenyl)-1H-phenanthro[9,10-d]imidazole

Tributyl(4-hexylthiophen-2-yl) stannane (560 mg, 1.20 mmol) and M2 (300 mg, 543 μmol) were dissolved in freshly distilled toluene. The mixture was bubbled with argon for an hour. Then bis(triphenylphosphine)palladium(II) chloride (19.06 mg, 27.16 μmol) and tri(o-tolyl) phosphine (49.60 mg, 163 μmol) were added in one

portion and mixture was stirred for fifteen minutes. The well dispersed mixture was refluxed at 120 °C for 7 hours. After completion of the coupling reaction, the solution was concentrated under vacuum. The residue was extracted by chloroform and organic layer was washed by brine two times. The organic layer was dried over sodium sulfate. The crude product was purified by column chromatography (1:20 ethyl acetate: petroleum ether) to give a viscous yellow oil (225 mg, 57%). ¹H NMR (400 MHz, CDCl₃) δ 8.77 (dd, J = 7.9, 0.9 Hz, 1H), 8.57 (t, J = 8.9 Hz, 1H), 8.52 (d, J = 8.3 Hz, 1H), 7.59 (t, J = 7.4 Hz, 1H), 7.52 – 7.43 (m, 1H), 7.32 (dt, J = 21.1, 7.0 Hz, 1H), 7.13 – 7.04 (m, 3H), 6.90 – 6.81 (m, 5H), 6.63 (s, 1H), 6.57 (d, J = 6.1 Hz, 1H), 6.51 (s, 1H), 2.42 – 2.36 (t, 2H), 2.25 (t, J = 7.6 Hz, 2H), 1.48 (ddd, J = 22.2, 11.4, 5.0 Hz, 4H), 1.33 – 1.11 (m, 14H), 1.09 – 0.92 (m, 8H), 0.85 – 0.62 (m, 11H).

2.12 Synthesis of 2-(5,5''-dibromo-4,4''-dihexyl-[2,2':5',2''-terthiophen]-3'-yl)-1-(4-fluorophenyl)-1H-phenanthro[9,10-d]imidazole

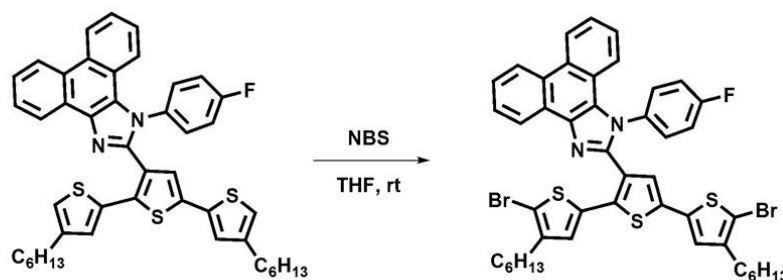


Figure 22. Synthesis of 2-(5,5''-dibromo-4,4''-dihexyl-[2,2':5',2''-terthiophen]-3'-yl)-1-(4-fluorophenyl)-1H-phenanthro[9,10-d]imidazole

2-(4,4''-Dihexyl-[2,2':5',2''-terthiophen]-3'-yl)-1-(4-fluorophenyl)-1H-phenanthro[9,10-d]imidazole (225 mg, 310 μmol) was dissolved in anhydrous THF. The solution was charged in aluminum foil sealed two neck flask by syringe and NBS (115 mg, 650 μmol) was added to solution portionwise in two hours. The reaction was completed after 8 hours and THF was removed. The crude product was purified by column chromatography (ethyl acetate: hexane 1:40) without extraction. The final product was a dark yellow oil (87 mg, 32%) named as M2. ¹H NMR (400 MHz, CDCl₃) δ 8.78 (d, J = 6.9 Hz, 1H), 8.73 (d, J = 8.3 Hz, 1H), 8.67 (d, J = 8.3 Hz, 1H),

7.69 (t, J = 7.1 Hz, 1H), 7.62 (dd, J = 11.1, 4.2 Hz, 1H), 7.48 (t, J = 7.1 Hz, 1H), 7.23 (t, J = 7.2 Hz, 1H), 7.14 (d, J = 7.5 Hz, 1H), 7.07 – 6.98 (m, 5H), 6.77 (s, 1H), 6.56 (s, 1H), 2.49 – 2.43 (m, 2H), 2.34 – 2.29 (m, 2H), 1.56 – 1.45 (m, 4H), 1.39 – 1.17 (m, 11H), 1.08 (ddd, J = 14.5, 12.3, 7.3 Hz, 6H), 0.83 (t, J = 7.1 Hz, 3H), 0.73 (t, J = 7.0 Hz, 3H). ¹³C NMR (101 MHz, CDCl₃) δ 145.85 – 145.37, 142.88, 137.65 – 137.12, 135.87 – 135.80, 135.36 – 135.33, 135.12, 134.06, 133.95, 133.30, 133.19, 129.65, 129.61, 129.52, 129.43, 129.33, 128.28, 128.26, 127.37, 127.25, 127.16, 126.97, 126.55, 126.30, 126.20, 125.75, 125.23, 125.17, 124.96, 124.12, 123.05, 122.72, 122.57, 122.47, 120.73, 116.55, 116.32, 110.38, 110.26, 108.64, 108.57, 31.40, 29.34, 28.72, 22.41, 13.96. HRMS, Mass: 885.0858, Calculated: 885.0845.

2.13 Synthesis of P1

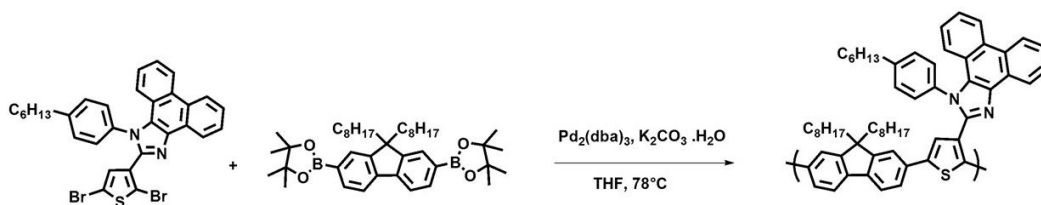


Figure 23. Synthesis of P1

K₂CO₃ was dissolved in deionized water to prepare 2 M, 1 mL solution. The solution was charged in 25 mL two neck round bottom flask and purged with argon for 30 min. Under argon atmosphere in a separate flask M1 (150 mg, 243 μmol) was dissolved in freshly distilled THF. After that, 2,2'-(9,9-dioctyl-9H-fluorene-2,7-diyl)bis(4,4,5,5-tetramethyl-1,3,2-dioxaboralane) (156 mg, 243 μmol) was added to the potassium carbonate solution, then the mixture was bubbled with argon for further 30 min. The ammonium tetrahexyl iodide (5.00 mg, 21.0 μmol) was added to mixture followed by purging for extra thirty minutes. After that, tris(o-tolyl)phosphine (29.5 mg, 97.0 μmol) and tris(dibenzylideneacetone) dipalladium(0) (11.0 mg, 12.10 μmol) was added to the solution. The polymerization reaction was refluxed at 80 °C for 60 hours under argon atmosphere. Then 2-bromothiophene (96.5 mL, 970 μmol) was added to mixture followed by addition of 3 mg

tris(dibenzylideneacetone) dipalladium(0) and 5 mg tris(o-tolyl)phosphine . After 4 hours, other end copper thiophene-2-boronic acid pinacol ester (204 mg, 970 μmol) was added to mixture followed by addition of 3 mg tris(dibenzylideneacetone) dipalladium(0) and 5 mg tris(o-tolyl)phosphine. The reaction was ended after 4 hours. After cooling to room temperature THF was removed under reduce pressure. The polymer solution was dissolved in 1 mL (0.5 mL, two times) and precipitate in 200 mL cold methanol. The precipitants were collected by vacuum filtration. For purification of the precipitants, Soxhlett apparatus was used. The precipitates were washed first by methanol followed by washing with acetone. The polymer was collected with hexane. After that, the solvent was removed under reduced pressure. The polymer was dissolved in 0.5 mL chloroform and precipitated in cold methanol. The precipitant was collected by vacuum filtration to give 130 mg (61%) **P1**. GPC results M_w : 10162, M_n : 7327 PDI:1.39

2.14 Synthesis of P2

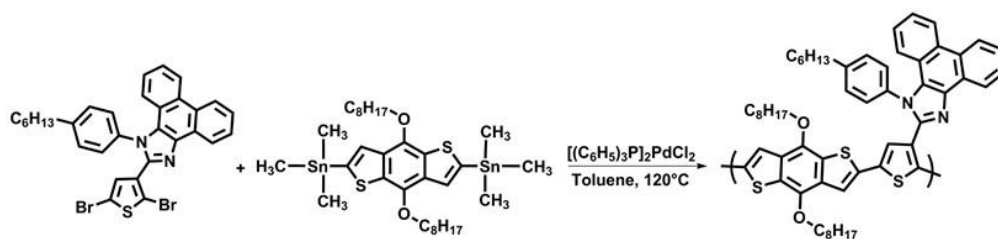


Figure 24. Synthesis of **P2**.

M1(160 mg, 259 μmol) was dissolved in 7 mL freshly distilled toluene under argon atmosphere. The solution was transferred to 25 mL two necked round bottom flask under argon. The solution was bubbled with argon for half an hour. After that, 4,8-bis(octyloxy)benzo[1,2-b:4,5-b'] dithiophene-2,6-diyl bis(trimethylstannane) (200mg, 259 μmol) was added and the mixture was degassed with argon for 30 min. Then bis(triphenylphosphine) palladium(II) chloride (9.10mg, 13 μmol) and tri(o-tolyl) phosphine (31 mg, 103 μmol) was added followed by refluxing the solution at 120°C for 60 hours. After completion of polymerization, 2-bromothiophene (100

mmL, 1.00 mmol), and additional 3 mg of bis(triphenylphosphine) palladium(II) chloride was added to solution. After four hours, tributyl(thiophen-2-yl) stannane (235 mmL, 1.00 mmol) was added to solution and the reaction continued for four more hours. After cooling to room temperature the solution was concentrated under reduced pressure. The polymer solution was dissolved in 1 mL (in 0.5 two time) and precipitated in 200 mL cold (4-5 °C) methanol. The precipitants were filtered collected residual purified with Soxhlet apparatus. First it was washed with methanol followed by washing with acetone to remove the catalyst and unreacted reactants. The oligomers were collected with hexane and the polymer was collected in chloroform. The polymer was precipitated in methanol after concentrating of the solution under reduced pressure to give 190mg (79%) **P2**. GPC results: M_w :58400 M_n : 31500. PDI: 1.86.

2.15 Synthesis of P3

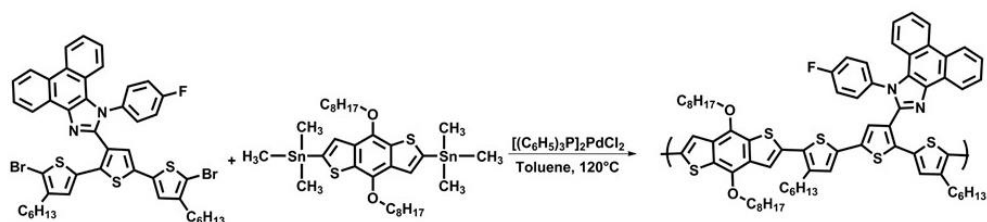


Figure 25. Synthesis of **P3**.

M2 (87.00 mg, 98.32 μ mol) was dissolved in 7 mL freshly distilled toluene under argon atmosphere. The solution was transferred to 25 mL two necked round bottom flask under argon. The solution was bubbled with argon for 30 min. After that, (4,8-bis(octyloxy)benzo[1,2-b:4,5-b'] dithiophene-2,6-diyl) bis(trimethylstannane) (76 mg, 98.0 μ mol) was added and bubbled for extra half an hour. Then bis(triphenylphosphine) palladium(II) chloride (3.50 mg, 4.92 μ mol) and tri(o-tolyl) phosphine (12.0 mg, 39.0 μ mol) was added followed by refluxing the solution at 120 °C for 60 hours. After completion of polymerization, 2-bromothiophene (38.0 mmL, 393 μ mol) and additional 3 mg of bis(triphenylphosphine) palladium(II) chloride was added to solution. After four hours tributyl(thiophen-2-yl) stannane (80 mmL, 394

μmol) was added to solution and the reaction continued for four more hours. After cooling to room temperature the solution was concentrated under reduced pressure. The polymer was dissolved in 1 mL (in 0.5 two times) and precipitated in 200 mL cold (4-5 °C) methanol. The precipitants were filtered collected residual purified with Soxhlet apparatus. First it was washed with methanol followed by washing with acetone to remove catalyst and unreacted reactants. The oligomers were collected in hexane and the polymer was collected in chloroform. The polymer was precipitated in methanol after concentrating the solution under reduced pressure. For extra purification the collected polymer was dissolved in chloroform and 5 mg quadrazine was added to it and stirred for 1 hour. The mixture was passed from silicon packed column in which chloroform was solvent. The solvent was removed under reduce pressure to give 53mg (45%) **P3**. GPC results: M_w :26600 Da, M_n : 16700 Da. PDI: 1.60.

2.16 Organic Photovoltaic Device Fabrication

The PV device was constructed according to the following procedure. The ITO was etched by hydrochloric acid. The film was cleaned by successive rinsing in toluene, distilled water with detergent, distilled water, acetone and isopropyl alcohol. For removing any organic contaminations ozone treatment was performed for 5 min. After cleaning the ITO, PEDOT: PSS was coated by spin coater (G3P-8) at rate of 5000 rpm. To removing solvent, the film was heated at 130 °C for 15 min. Then chloroform was used to prepared polymer-PCBM solution. The solution passed through 0.22 μm PTFE membrane. The solution was spin coated in a glove box. The spinning rpm was 750 for the first 30 seconds then the rate was increased to 2500 for 40 seconds. Lithium fluoride (LiF) was (1 nm) physically evaporated on polymer in glove box under inert atmosphere (the pressure was below 10^{-6} mbar and the concentration of O_2 and H_2O were below 1ppm). Lastly aluminum electrode was evaporated on top of the calcium layer by rate of 0.1 \AA per second in an inert atmosphere. The J-V charectrization of the device was investigated by Keithley SMU 236 as source in glove box via 1.5 G illuminance (100 mV/cm).

2.17 OLED Device Fabrication

For preparing OLED device, ITO was cleaned as mention before. The PEDOT:PSS was coated by spin coater at a rate of 5000 rpm. To removing solvent, the film was heated at 130 °C for 15 min. The corresponding polymer was dissolved in chloroform and the solution was passed through 0.22 μm PTFE membrane. Then the filtered solution spin coated on top of PEDOT:PSS at rate of 2000 rpm for 40 seconds. The LiF about 1 nm was physically evaporated in on top of polymer layer. Lastly aluminum about 100 nm was evaporated at rate of 0.5-0.1 \AA per second in inert atmosphere.

CHAPTER 3

Results and discussion

3.1 Synthesis

Recent advances in organic synthesis utilizing cross coupling reaction become driving force in field of polymer based optoelectronic applications. In this work two monomers were synthesized and polymerized via Suzuki and Stille coupling reactions. Firstly, thiophene-3-carbaldehyde was brominated in ice cold condition to synthesize 2,5-dibromothiophene-3-carbaldehyde. Then, monomers were synthesized from 2,5-dibromothiophene-3-carbaldehyde, ammonium acetate, phenanthrene-9,10-dione and corresponding aniline (4-hexylaniline or 4-fluoroaniline) which result in imidazole ring closure [47,48]. 4-hexylaniline containing moiety donated as monomer 1 (M1). M1 and 2,2'-(9,9-Dioctyl-9H-fluorene-2,7-diyl)bis[4,4,5,5-tetramethyl-1,3,2-dioxaborolane] alternately polymerized via Suzuki polycondensation reaction to synthesize **P1**. Also, M1 polymerized with 4,8-bis(octyloxy)benzo[1,2-b:4,5-b'] dithiophene-2,6-diyl bis(trimethylstannane) in presence of palladium(II) catalysts to synthesize **P2**. However, 4-fluoroaniline containing moiety has low solubility, hence, this moiety coupled with tributyl(4-hexylthiophen-2-yl)stannane as bridge. This bridge not only increase the solubility but also expected to increase the planarity and conjugation path. After coupling with thiophene bridge, it was brominated from bridge sides to synthesize monomer 2 (M2). M2 polymerized with 4,8-bis(octyloxy)benzo[1,2-b:4,5-b'] dithiophene-2,6-diyl bis(trimethylstannane) via Stille coupling reaction which named as **P3**.

3.2 Cyclic voltammetry

The electronic band gap of polymers can be determined by cyclic voltammetry. Besides the location of HOMO and LUMO of polymers can be calculated by means of CV. To investigate electronic properties of the polymers in thin film on ITO they were prepared by spray coating from chloroform (5 mg/mL) solution. The voltammetry studies were conducted in a three electrode system in which acetonitrile and TBAPF₆ were the solvent and the supporting electrolyte respectively. In this system, polymer coated ITO was the working electrode, a platinum wire was the counter electrode and a silver wire was the reference one. In this experiment voltage was scanned with a rate of 100 mV/s in all cases. From results of electrochemical studies LUMO and HOMO energy levels were calculated using onset potentials of reduction and oxidation peaks. These calculations are shown in equations 13 and 14.

$$\text{HOMO} = -(4.75 + E_{\text{onset}}^{\text{ox}}) \quad \text{Equation 13}$$

$$\text{LUMO} = -(4.75 + E_{\text{onset}}^{\text{red}}) \quad \text{Equation 14}$$

The cyclic voltammetry spectra of polymers are shown in **Figure 28**. As can be seen from **Figure 28**, **P1** shows only oxidation potential at 1.59 V with reversible reduction peak at 1.27 V. Likewise, **P2** shows only oxidation potential at 1.20 V and dedoping peak at 0.72 V. However, **P3** shows ambipolar characteristics. The p-type and n-type reversible oxidation and reduction pairs of **P3** were observed as 1.10/0.79 V and -0.91/-0.78 V respectively.

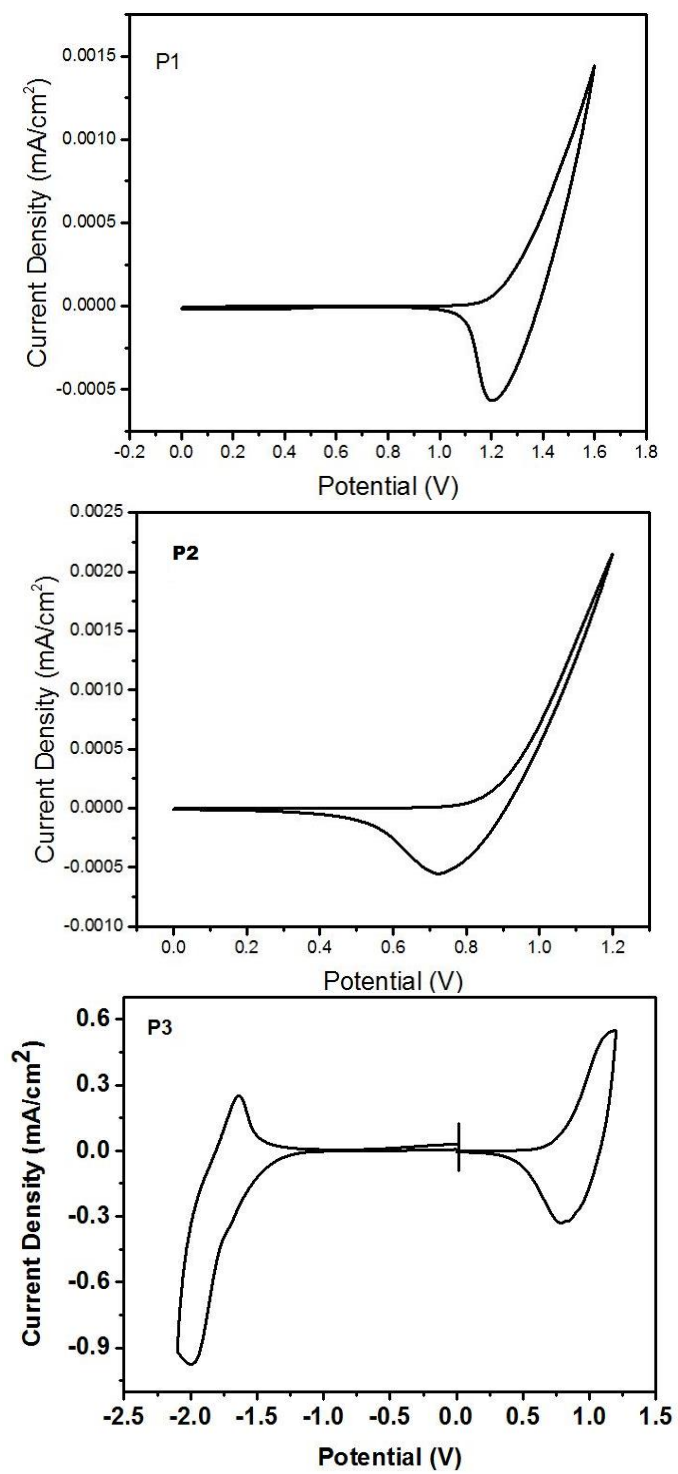


Figure 26. Cyclic Voltammetry of P1, P2 and P3

The HOMO of polymers was measured from oxidation onset. However, the LUMO of **P1** and **P2** could not be measured directly. HOMO of **P1** and **P2** were calculated as -6.00 and -5.64 eV respectively. Hence, LUMO of these two polymer calculate from E_g^{op} and HOMO. The calculated LUMO of **P1** is -3.6 eV and LUMO of **P2** calculate as -3.42 eV. Since **P3** is - ambipolar, the band gap of polymers can be calculated from CV directly. The measured HOMO from onset of oxidation peak is - 5.53 eV for **P3**. The LUMO was calculated as -3.09 eV. For **P3**. From difference of HOMO and LUMO levels of corresponding polymer electronic band gap (E_g^{ec}) calculated as 2.44 eV for **P3**. These results are summarized in **Table 1**.

Table 1. Electrochemical Characteristics of Polymers.

	$E_{p-doping}$ (V)	$E_{p-dedoping}$ (V)	$E_{n-doping}$ (V)	$E_{n-dedoping}$ (V)	HOMO (eV)	LUMO (eV)	E_g^{ec} (ev)
P1	1.60	1.20			-6.00	-3.6	
P2	1.22	0.72			-5.64	-3.42	
P3	1.10	0.78	-2.03	-1.67	-5.53	-3.09	2.44

3.3 Spectroelectrochemical Studies

Spectroelectrochemical experiments were conducted to investigate the optical properties of polymers during redox reactions. In this study, polymer films were prepared by spray coating on ITO from polymer solution (5mg/mL in chloroform). The films were connected to the three electrode system in which acetonitrile and TBAPF₆ were the solvent and the supporting electrolyte respectively. The spectroelectrochemical spectra of the **P3** in Uv-Vis-NIR region is depicted in **Figure 29**. The first absorption peak in spectrum where polymers are completely in their neutral state correspond to $\pi-\pi^*$ transition in visible region. Upon applying potential absorbance of neutral state of polymer depletes whereas intensities of oxidized form

of polymer with lower band gap known as polaron and bipolaron bands increase (shown by arrow in the spectra). The maximum absorption in neutral state was observed as 465 nm for **P3**. **P3** showed maximum peaks for polaron and bipolaron band at 740 and 1700 nm respectively. The color of **P3** is red in neutral and by oxidation the color of it changes to light grey at 1 V and fully oxidation form at 1.1 V shows dark grey color. The reduced form of the **P3** reveal marine color. The resulting color of polymers are represented **Figure 29**.

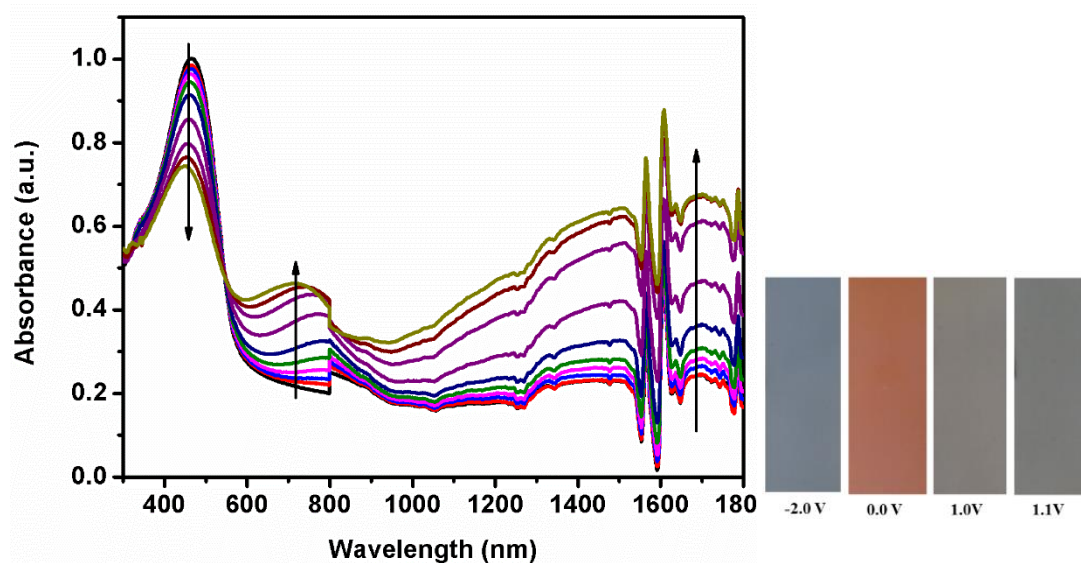


Figure 27. Spectroelectrochemical Spectra of **P3** and color at -2, 0, 1 and 1.1 V.

3.4 Kinetic Studies

In order to measure switching times and optical contrast of polymers between their neutral state and oxidized state kinetic studies were performed. To do this, a potential was applied to the polymer coated ITO film with a residence time of 5 seconds for each cycle. During this experiment voltage was changed between 0.0-1.1V for **P3** in defined time interval and the percent transmittance was measured in visible and near IR regions. The results are depicted in **Figure 30** and the switching time and optical contrasts are represented in **Table 2**. The optical contrast of **P3** was measured as 8%

at 465 nm, 14% at 740 nm and 55% at 1700 nm. The time that is necessary to reach 95% change in transmittance during applied potential is called switching time. The observed switching times for **P3** are 3.6, 0.6 and 1.0 s at 465, 740 and 1700 nm respectively. The reason for high switching time for polymers may be the transport resistance of counter ion, lack of porosity of polymers and compact aggregation of the film which prevents counter ion penetration [50].

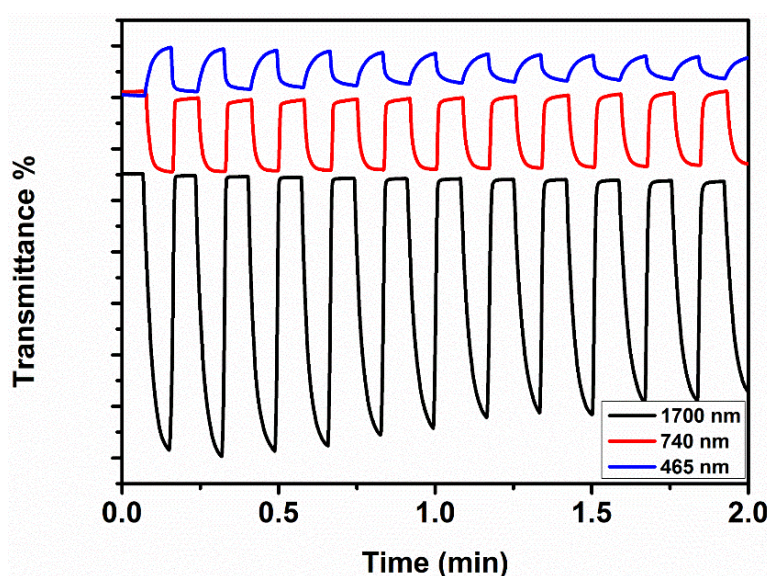


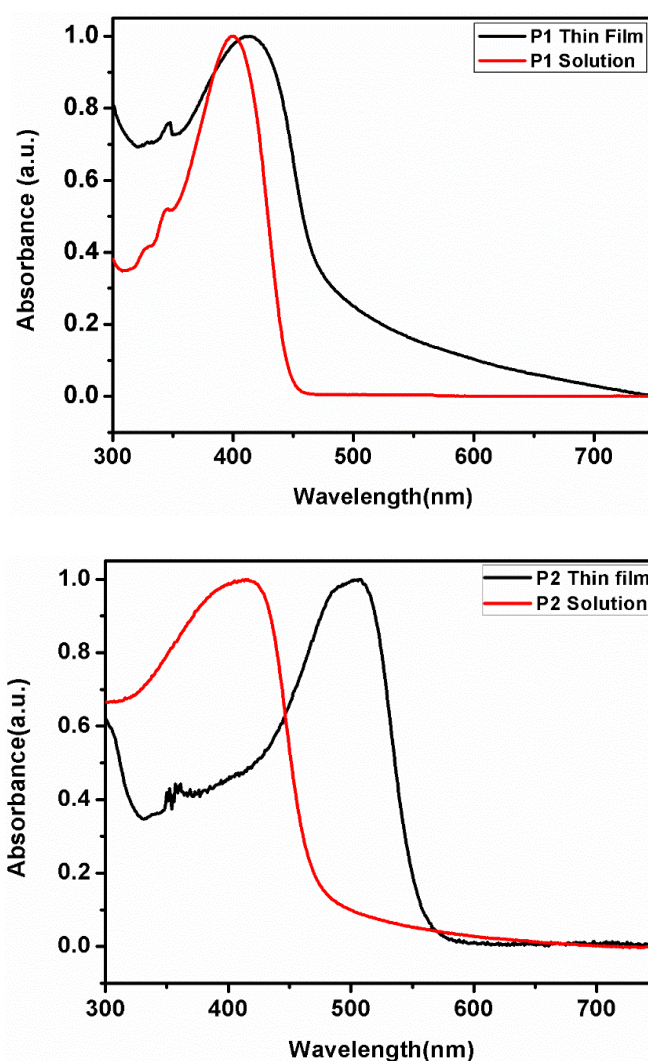
Figure 28. Percent Transmittance Change of **P3**.

Table 2. Switching Times and Optical Contrast in Near IR and Visible region

	Wavelength(nm)	Optical Contrast($\Delta T\%$)	Switching Times (s)
P3	1700	55	1.0
	740	14	0.6
	465	8	3.6

3.5 Optical Properties of Polymers

Optical properties of polymers were investigated via UV-visible absorption spectroscopy. The measured absorption spectra of polymers are presented in **Figure 31**. The onset, maxima and optical band gap of the polymers are represented in **Table 3**. The maxima were observed for **P1**, **P2** and **P3** as 410, 508 and 456 nm respectively. Via incorporating a bridge to polymer back bone, it is expected to have a lower band gap with help of increasing planarity and conjugation path. The optical band gap of the **P3** which contains thiophene bridge is smaller than **P1** and **P2** as expected.



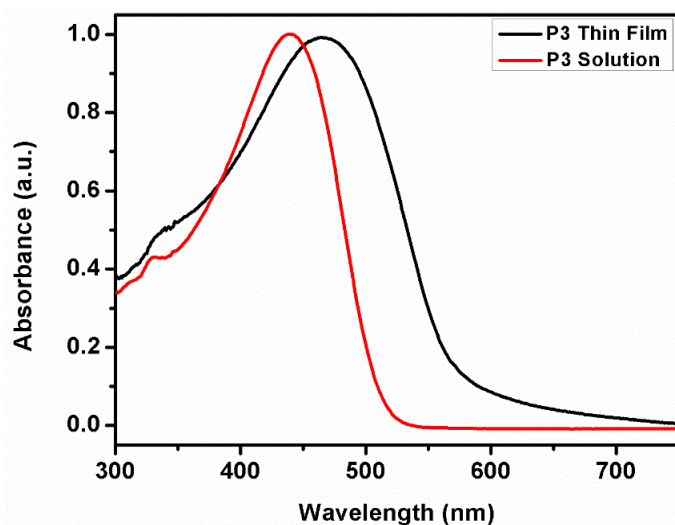


Figure 29. Uv-Visible Absorption Spectra of the Polymers (**P1**, **P2** and **P3**) in chloroform Solution and thin film.

Table 3. Optical Properties of Polymer.

	λ_{\max} (nm)	$\lambda_{\max}^{\text{onset}}$ (nm)	E_g^{op} (eV)
P1	410	520	2.40
P2	508	560	2.22
P3	465	568	2.18

3.6 Thermal Analysis of Polymers

The thermal properties of polymers were investigated by DSC and TGA. The TGA results show glass transition of **P1** at 128 °C and for **P2** the glass transition could not be determined which can be attributed to the rigidity of polymer structure. The DSC results show that **P1** weight loss of 48% at 430 °C and continue to weight loss of 53% until 657 °C. **P2** is stable up to 320 °C and weight loss of 38.4% is seen until 700 °C. (All results are in Appendix B).

3.7 Polymer Light Emitting Diode Application of P1

In this study OLED properties of **P1** was investigated. The luminescence of polymer was investigated through photoluminescence and electroluminescence. In order to study the photoluminescence characteristics both solution and thin film were excited at corresponding maximum absorptions. The maximum emission of the polymer in chloroform solution was 425 nm and 485 nm in thin film (**Figure 32**). The red shift in thin film can be explained by the stacking of molecules and lower degree of freedom in compare to those in solution.

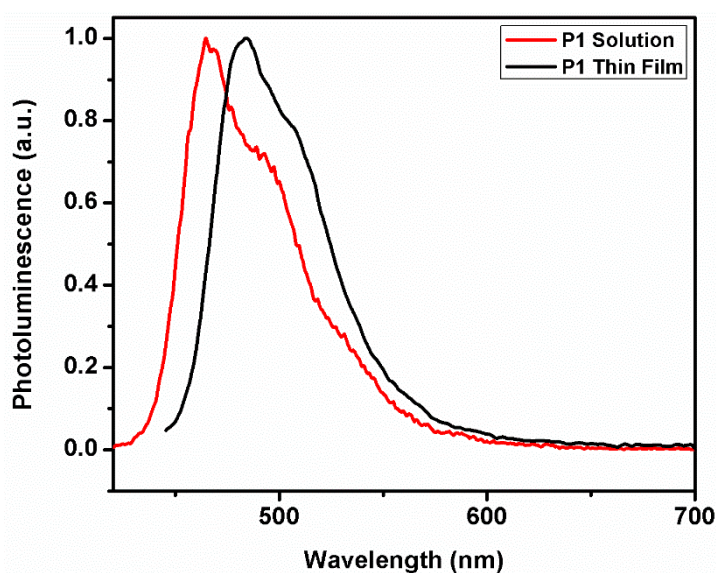


Figure 30. Photoluminescence of **P1** in chloroform solution and thin film.

In order to measure electroluminescence and current density-luminescence-voltage characteristics (JLV) of a single layer device with ITO/PEDOT:PSS/**P1**/LiF/Al structure was constructed. The device has a turn on voltage of 11 V with a luminescence of 210 cd/m² and represents maximum luminescence of 5627 cd/m² at 13V and 1267 mA/cm² as given in **Figure 33**. The electroluminescence spectrum of the polymer is shown in **Figure 34** which indicated maximum emission at 476 nm.

The high turn on voltage of the polymer can be correlated to the wide band gap which is vital for blue emission.

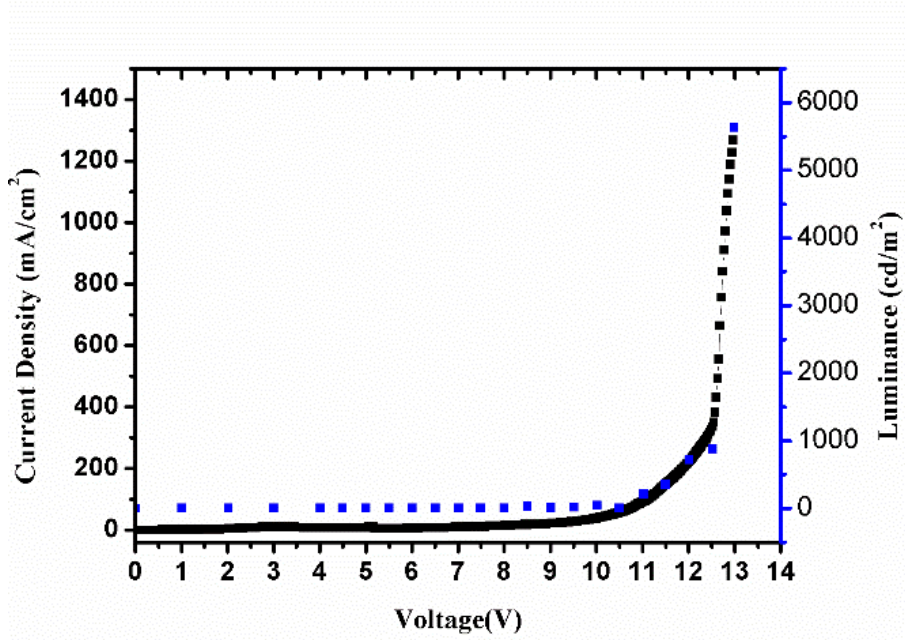


Figure 31. P1. JLV Characteristics of P1 with Maximum Luminescence at 13 V and 1267 mA/cm².

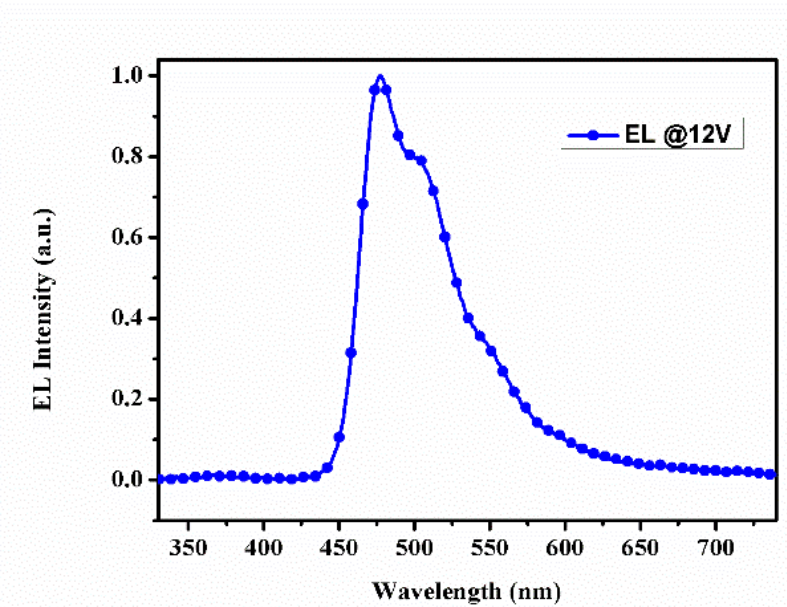


Figure 32. The Electroluminescence of P1 at 12 V and maximum emission of 476 nm.

The CIE coordinates of the emitted light were recorded as $x=0.187, y=0.369$ which correspond to greenish-blue color as seen in **Figure 35**.

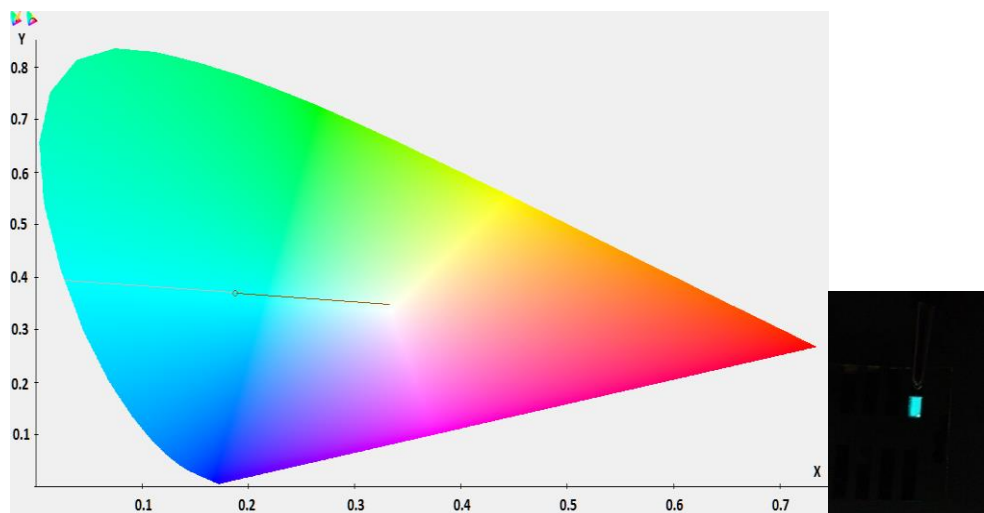


Figure 33. Color Coordinates of Emitted Light by **P1**.

3.8 Organic Photovoltaic Application

The photovoltaic properties of **P2** and **P3** were investigated with a device structure of ITO/PEDOT:PSS/Polymer:PCBM/LiF/Al under AM 1.5 condition in an inert atmosphere. The corresponding polymer was mixed with different ratios of PCBM to optimize active layer. The optimization results of polymer are represented in **Table 4**. The J - V characteristics of **P2** and **P3** are depicted in **Figure 36**. The best result for **P2** device was the 1:3 ratio of the polymer and PCBM with PCE of 0.94 % and 31% fill factor. The corresponding short current density and open circuit voltage of the device were measured as 5.62 mA/cm^2 and 0.54 V. The highest efficiency of **P3** was measured as 0.91% with 1:2 ratio of polymer:PCBM. The J_{sc} , V_{oc} and fill factor of **P3** device in this configuration were found as 4.48 mA/cm^2 , 0.58 V and 35% respectively. Although the open circuit voltages of the two polymers are all most same, **P2** shows 0.03% which can be attributed to higher short current density. On

the other hand, **P3** shows a fill factor of 35% which means the hole and electron transfer in this device more efficient than **P2**.

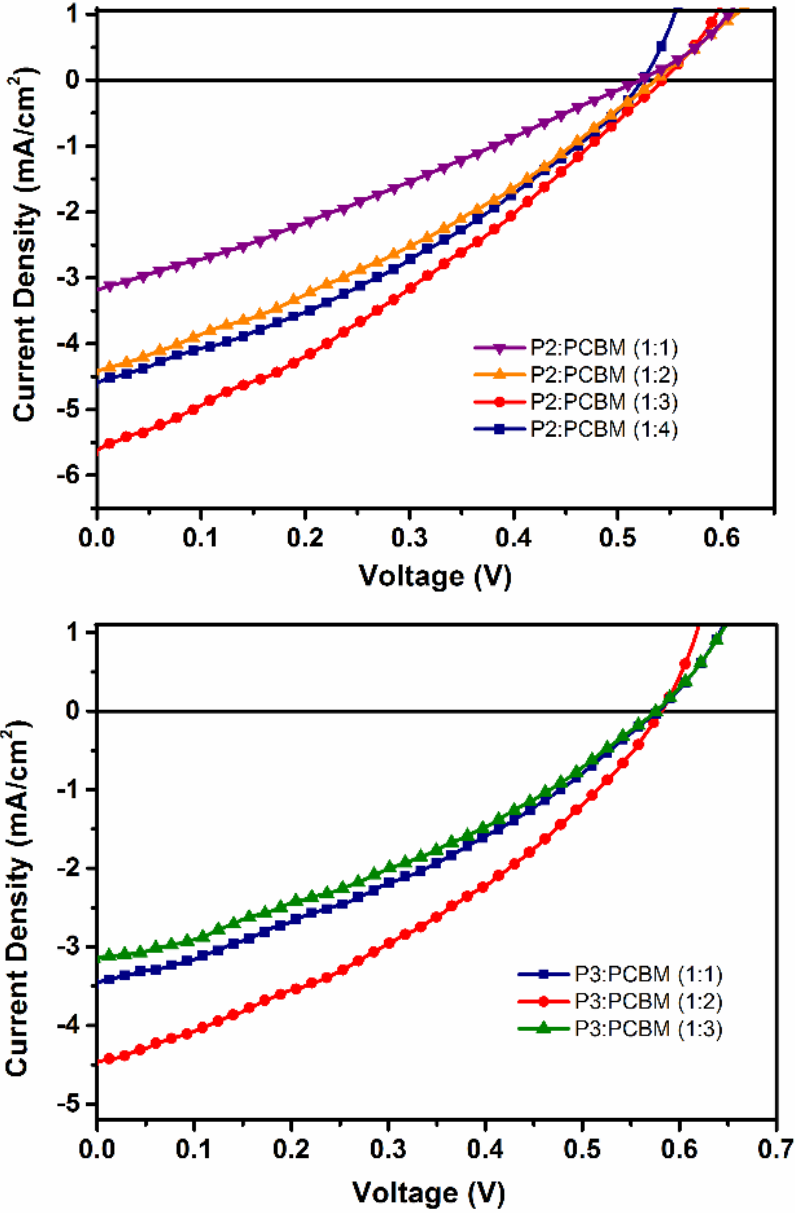


Figure 34. J-V characteristics of P2 and P3

Table 4. Optimization Studies of **P2** and **P3** for OPVs.

	P2:PCBM	V _{oc} (V)	J _{sc} (mA/cm ²)	V _{max} (V)	J _{max} (mA/cm ²)	FF (%)	PCE (%)
P2	1:1	0.52	3.19	0.28	1.68	28	0.47
	1:2	0.53	4.42	0.32	2.39	33	0.77
	1:3	0.54	5.62	0.30	3.16	31	0.94
	1:4	0.52	4.61	0.29	2.79	34	0.82
P3	1:1	0.57	3.49	0.33	2.04	34	0.67
	1:2	0.58	4.48	0.35	2.62	35	0.91
	1:3	0.57	3.13	0.34	1.82	35	0.62

CHAPTER 4

Conclusion

Three new conjugated polymers based on phenanthro-imidazole were synthesized via Suzuki and Stille coupling polycondensation reactions. These polymers were utilized as an active layer for organic photovoltaic and organic light emitting diode applications. Cyclic voltammetry, spectroelectrochemical and kinetic studies were conducted to investigate electrochromic and electrochemical properties of polymers. Electrochemical studies reveal that **P3** has ambipolar character with band gap of 2.44 eV. The optical band gap of the polymers were determined as 2.40, 2.22 and 2.18 eV for **P1**, **P2** and **P3** respectively. Kinetic studies represent **P3** could be promising candidate for near IR electrochromic devices due to its 55% optical contrast at 1700 nm with 1s switching time. **P1** shows a maximum luminescence of 5627 cd/m² at 13V and turn on voltage of 11V. The color coordination of CIE diagram was x=0.187, y=0.369 indicating cyan color. For **P2** and **P3** device optimizations were performed according to polymer and PC₇₁BM ratios. The optimized device of **P2** shows PCE of 0.94% , V_{oc} of 0.54V, J_{sc} of 5.63 mA/cm² and Fill Factor (FF) of 31%. The best performance of **P3** based device represent a PCE of 0.91%, V_{oc} of 0.58V, J_{sc} of 4.48 mA/cm² and Fill Factor (FF) of 35%.

REFERENCES

- [1] M.A.Green, K.Emery, Y.Hishikawa, W.Warta, E.D.Dunlop, *Prog. Photov. Res. Appl.* 24 (2016) 905–013.
- [2] P. Chapin, M, Fuller, C, G, *J. Appl. Phys.* 25 (1954) 675-682.
- [3] V.C. Sundar, J. Zaumseil, V. Podzorov, E. Menard, R.L. Willett, T. Someya, M.E. Gershenson, J. A. Rogers, *Science*. 303 (2004) 1644–1646.
- [4] W. Hu, *Organic Electronics II Organic Photovoltaics Physics of Organic Semiconductors Physical and Chemical Aspects of Organic Electronics* (2012) 526-527.
- [5] J. Zhao, Y. Li, G. Yang, K. Jiang, H. Lin, H. Ade, W. Ma, H. Yan, *Nat. Energy* 1 (2016) 15027-15034.
- [6] O.A. Abdulrazzaq, V. Saini, S. Bourdo, E. Dervishi, A.S. Biris, *Part. Sci. Technol.* 31 (2013) 427–442.
- [7] S. Kappaun, C. Slugovc, E.J.W. List, *Int. J. Mol. Sci.* 9 (2008) 1527–1547.
- [8] J.H. Burroughes, D.D.C. Bradley, A.R. Brown, R.N. Marks, K. Mackay, R.H. Friend, P.L. Burns, A.B. Holmes, *Nature* 347 (1990) 539–541.
- [9] W.M. Kline, R.G. Lorenzini, G.A. Sotzing, *Color. Technol.* 130 (2014) 73–80.
- [10] D. Rosseinsky, R.J. Mortimer, *Adv. Mater* 13 (2001) 783–793.
- [11] S.K. Deb, *Appl. Opt.* 8 (1969) 192-195.
- [12] R.J. Mortimer, *Electrochim. Acta* 44 (1999) 2971–2981.
- [13] A.A. Argun, P.H. Aubert, B.C. Thompson, I. Schwendeman, C.L. Gaupp, J. Hwang, N.J. Pinto, D.B. Tanner, A.G. MacDiarmid, J.R. Reynolds, *Chem. Mater.* 16 (2004) 4401–4412.
- [14] S. Sindhu, K. Narasimha Rao, S. Ahuja, A. Kumar, E.S.R. Gopal, *Mater. Sci.*

- Eng. B Solid-State Mater. Adv. Technol. 132 (2006) 39–42.
- [15] G. Sonmez, H. Meng, F. Wudl, Chem. Mater. 16 (2004) 574–580.
- [16] H. Shirakawa, E.J. Louis, A.G. MacDiarmid, C.K. Chiang, A.J. Heeger, J. Chem. Soc. Chem. Commun. (1977) 578–580.
- [17] J. Bredas, G. Street, Acc. Chem. Res. 1305 (1985) 309–315.
- [18] H. Winokur, M. Moon, Y. Heeger, Barker, J. Bott, D., Shirakawa, Phys. Rev. Lett. 59 (1987) 608-611.
- [19] Y.-W.P. D. Moses, J. Chen, A. Denenstien, M. Kaveh, T.-C. Chung, A.J. Heeger, A.G. MacDiarmid, Solid State Commun. 40 (1981) 1007–1010.
- [20] D. Jacquemin, C. Adamo, J. Chem. Theory Comput. 7 (2011) 369–376.
- [21] P. von R. Schleyer, Chem. Rev. 101 (2001) 1115-1117.
- [22] J. Roncali, Macromol. Rapid Commun. 28 (2007) 1761–1775.
- [23] C. Liu, K. Wang, X. Gong, A.J. Heeger, Chem. Soc. Rev. (2016) 4825 -4846.
- [24] S.Y. Leblebici, T.L. Chen, P. Olalde-Velasco, W. Yang, B. Ma, ACS Appl. Mater. Interfaces 5 (2013) 10105–10110.
- [25] O. V Mikhnenko, P.W.M. Blom, T.-Q. Nguyen, Energy Environ. Sci. 8 (2015) 1867–1888.
- [26] K. Feron, W.J. Belcher, C.J. Fell, P.C. Dastoor, Int. J. Mol. Sci. 13 (2012) 17019–17047.
- [27] V.D. Mihailetchi, H. Xie, B. De Boer, L.J.A. Koster, P.W.M. Blom, Adv. Func. Mater. 16 (2006) 699–708.
- [28] M. Kuik, G.-J. a H. Wetzelaer, H.T. Nicolai, N.I. Craciun, D.M. De Leeuw, P.W.M. Blom, Adv. Mater. 26 (2014) 512–31.
- [29] Z. Zhang, J. Wang, J. Mater. Chem. 22 (2012) 4178.
- [30] L. Lu, T. Zheng, Q. Wu, A.M. Schneider, D. Zhao, L. Yu, Chem. Rev. 115

(2015) 12666–12731.

- [31] M.C. Scharber, N.S. Sariciftci, *Prog. Polym. Sci.* 38 (2013) 1929–1940.
- [32] E. Bundgaard, F.C. Krebs, *Sol. En. Mater. Sol. Cells* 91 (2007) 954–985.
- [33] L. Dou, Y. Liu, Z. Hong, G. Li, Y. Yang, *Chem. Rev.* 115 (2015) 12633–12665.
- [34] S.R. Forrest, *MRS Bull.* 30 (2005) 28–32.
- [35] C. Brabec, V. Dyakonov, U. Scherf, *Organic Photovoltaics: Materials, Device Physics, and Manufacturing Technologies*, 2009.
- [36] M.C. Scharber, D. Mühlbacher, M. Koppe, P. Denk, C. Waldauf, A.J. Heeger, C.J. Brabec, *Adv. Mater.* 18 (2006) 789–794.
- [37] H. Li, M. Fang, Y. Hou, R. Tang, Y. Yang, C. Zhong, Q. Li, Z. Li, *ACS Appl. Mater. Interfaces* (2016) 12134-12140.
- [38] J. Hou, T.L. Chen, S. Zhang, L. Huo, S. Sista, Y. Yang, *Macromolecules* 42 (2009) 9217–9219.
- [39] B. Qi, J. Wang, *J. Mater. Chem.* 22 (2012) 24315.
- [40] N.K. Elumalai, A. Uddin, *Energy Environ. Sci.* 9 (2016) 391–410.
- [41] D. Gupta, S. Mukhopadhyay, K.S. Narayan, *Sol. En. Mater. Sol. Cells* 94 (2010) 1309–1313.
- [42] Y.-L. Chang, *Efficient Organic Light-Emitting Diodes (OLEDs)*, 2016.
- [43] N.H. Kim, Y.H. Kim, J.A. Yoon, S.Y. Lee, D.H. Ryu, R. Wood, C.B. Moon, W.Y. Kim, *J. Lumin.* 143 (2013) 723–728.
- [44] N. Thejo Kalyani, S.J. Dhoble, *Renew. Sustain. Energy Rev.* 16 (2012) 2696–2723.
- [45] W. Brütting, J. Frischeisen, T.D. Schmidt, B.J. Scholz, C. Mayr, *Phys. Status Solid Appl. Mater. Sci.* 210 (2013) 44–65.

- [46] E. Efstathios, *Green Energy and Technology*, 2006.
- [47] Y. Zhang, S.-L. Lai, Q.-X. Tong, M.-Y. Chan, T.-W. Ng, Z.-C. Wen, G.-Q. Zhang, S.-T. Lee, H.-L. Kwong, C.-S. Lee, *J. Mater. Chem.* 21 (2011) 8206-8214.
- [48] Y. Te Chang, S.L. Hsu, M.H. Su, K.H. Wei, *Adv. Func. Mater.* 17 (2007) 3326–3331.
- [49] P. Cheng, Y. Li, X. Zhan, *Energy Environ. Sci.* 7 (2014) 2005 1351-1356.
- [50] Z. Shi, W.T. Neo, T.T. Lin, H. Zhou, J. Xu, *RSC Adv.* 5 (2015) 96328–96335.

Appendix A

NMR RESULTS

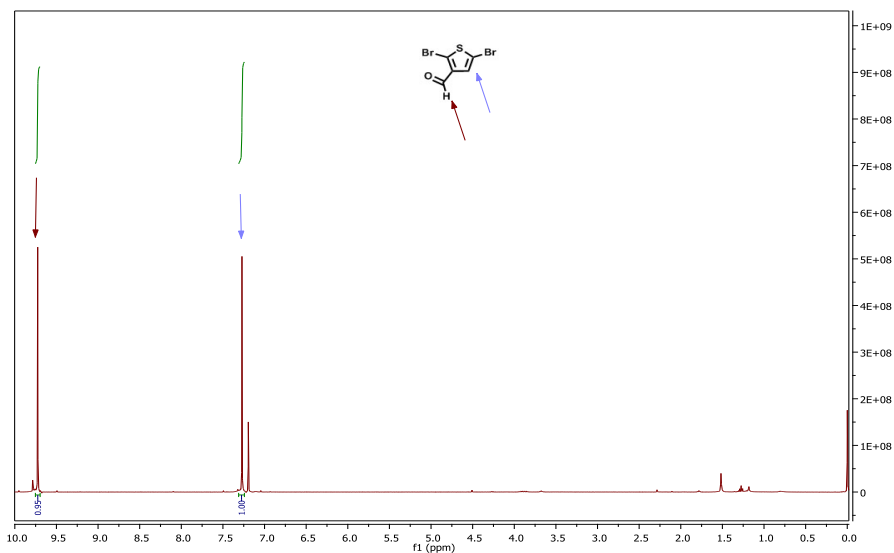


Figure 35. ^1H NMR of 2,5-dibromothiophene-3-carbaldehyde

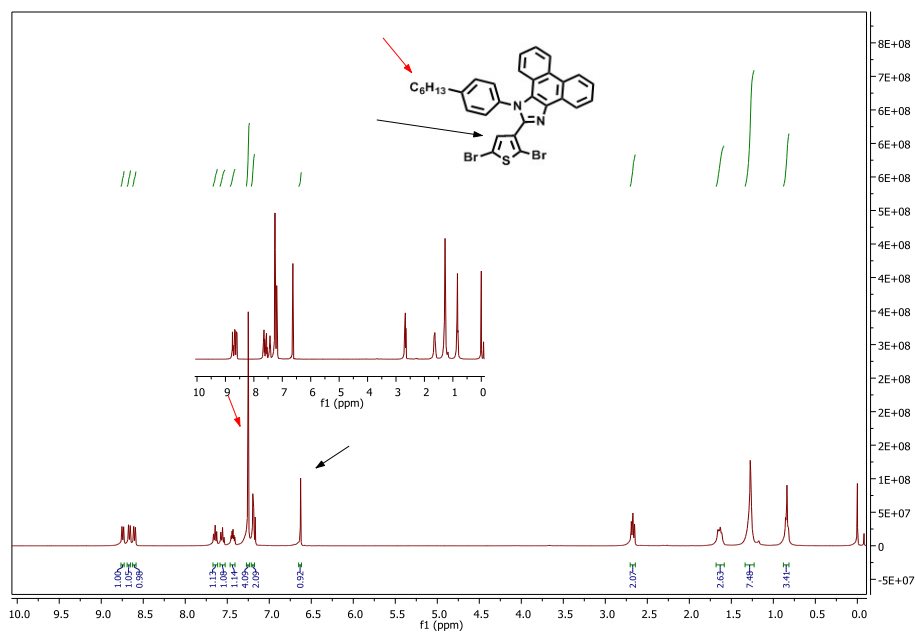


Figure 36. ^1H NMR of 2-(2,5-dibromothiophen-3-yl)-1-(4-hexylphenyl)-1H-phenanthro[9,10-d]imidazole

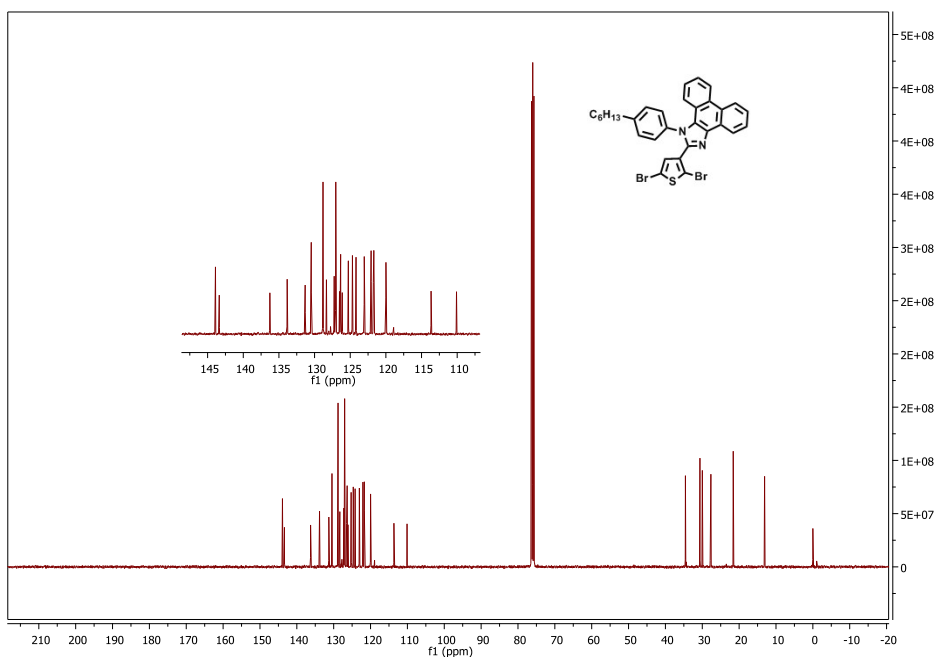


Figure 37. ^{13}C NMR of 2-(2,5-dibromothiophen-3-yl)-1-(4-hexylphenyl)-1H-phenanthro[9,10-d]imidazole

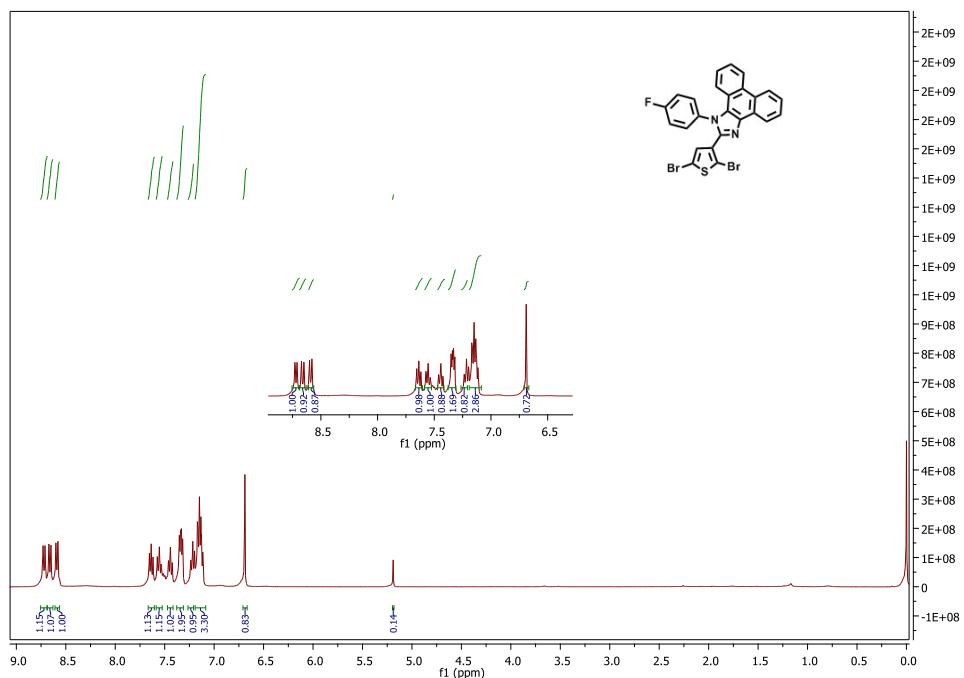


Figure 38. ^1H NMR of 2-(2,5-dibromothiophen-3-yl)-1-(4-fluorophenyl)-1H-phenanthro[9,10-d]imidazole

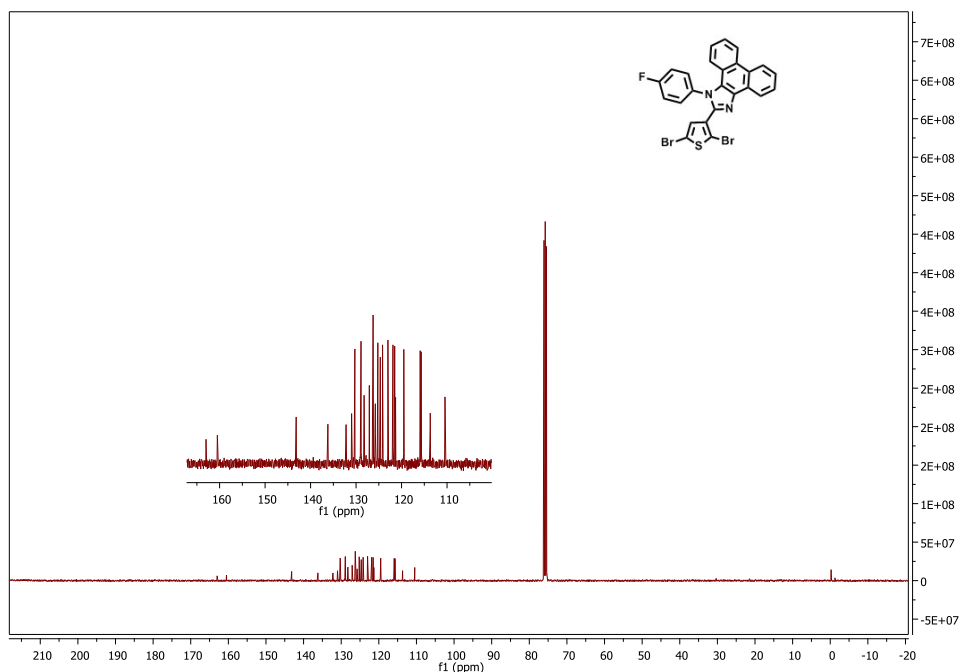


Figure 39. ^{13}C NMR of 2-(2,5-dibromothiophen-3-yl)-1-(4-fluorophenyl)-1H-phenanthro[9,10-d]imidazole

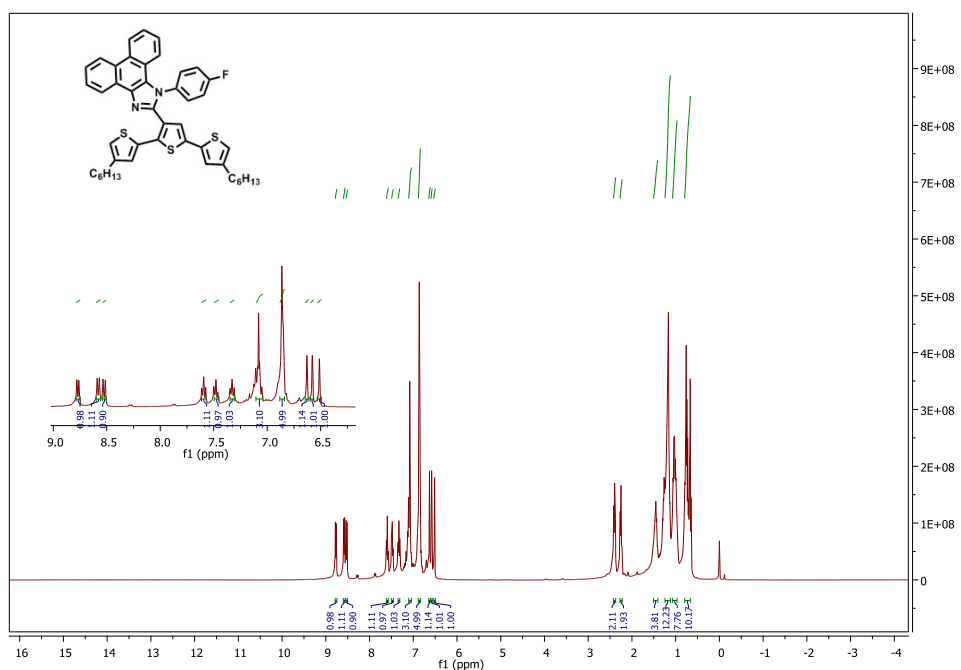


Figure 40. ^1H NMR of 2-(4,4''-dihexyl-[2,2':5',2''-terthiophen]-3'-yl)-1-(4-fluorophenyl)-1H-phenanthro[9,10-d]imidazole

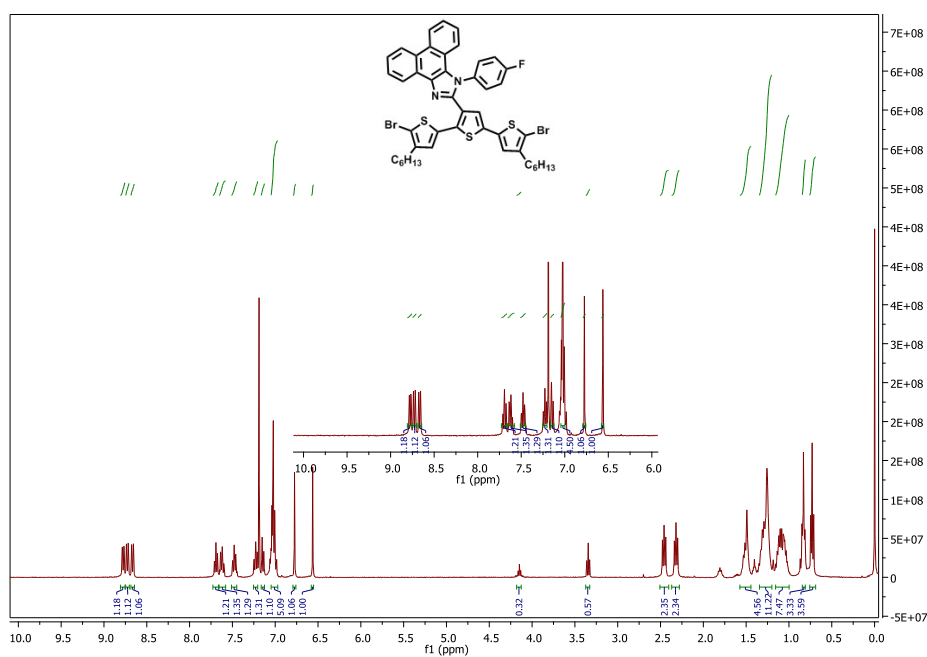


Figure 41. ^1H NMR of 2-(5,5''-dibromo-4,4''-dihexyl-[2,2':5',2''-terthiophen]-3'-yl)-1-(4-fluorophenyl)-1H-phenanthro[9,10-d]imidazole

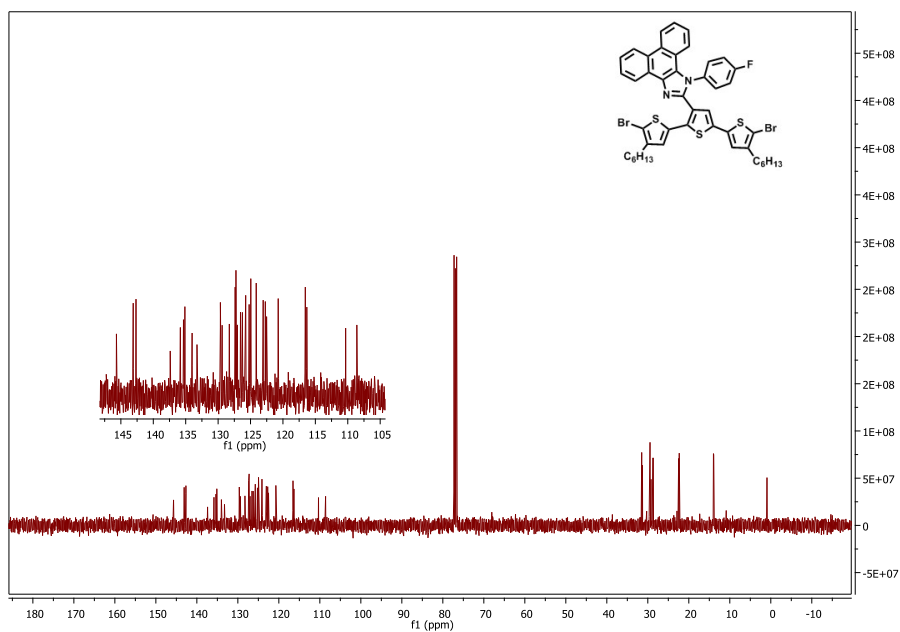


Figure 42. ^{13}C NMR of 2-(5,5''-dibromo-4,4''-dihexyl-[2,2':5',2''-terthiophen]-3'-yl)-1-(4-fluorophenyl)-1H-phenanthro[9,10-d]imidazole.

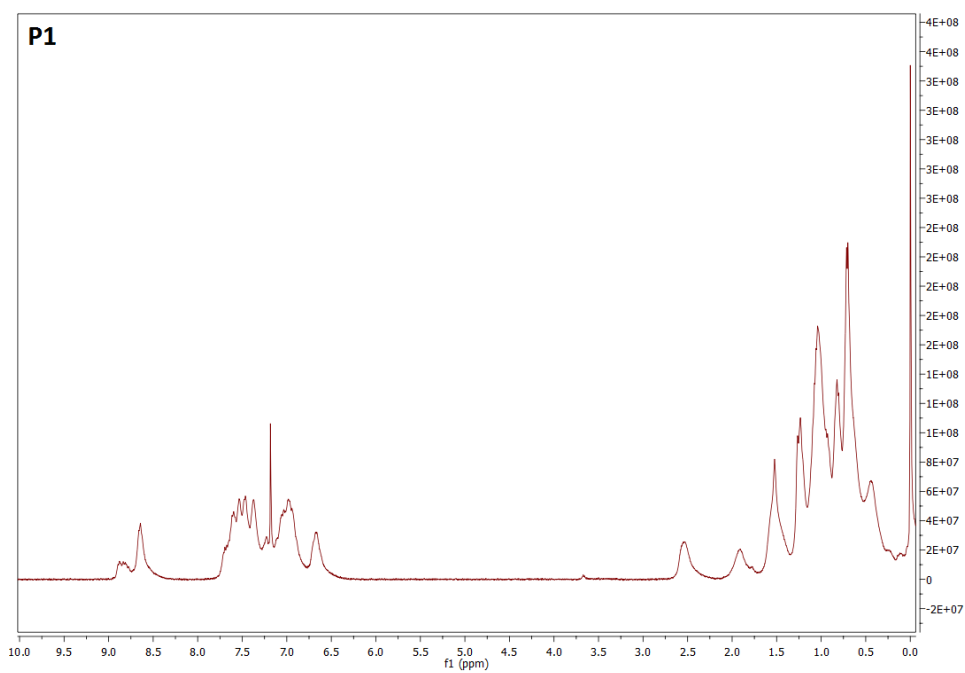


Figure 43. ^1H NMR of P1.

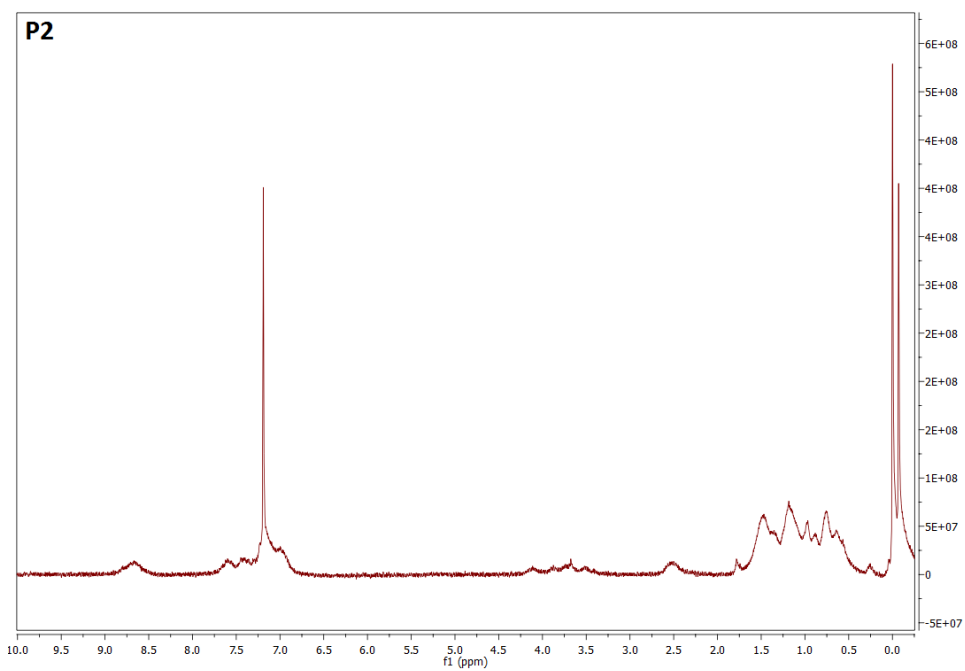


Figure 44. ^1H NMR of P2.

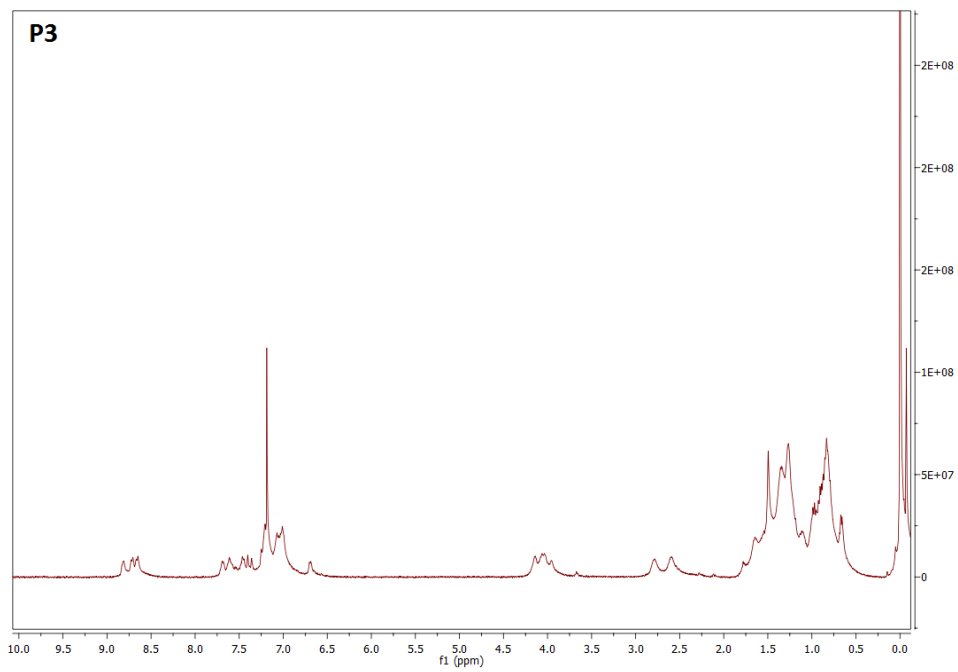


Figure 45. ^1H NMR of P3.

Appendix B

Thermal Analysis Results

1. Numune: 18147-1

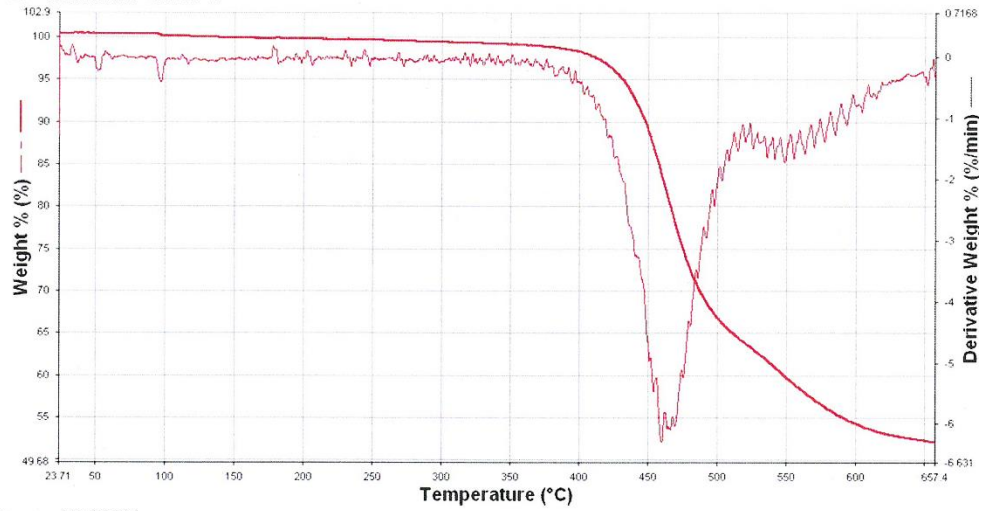


Figure 46. DSC Thermogram of P1.

2. Numune: 18147-2

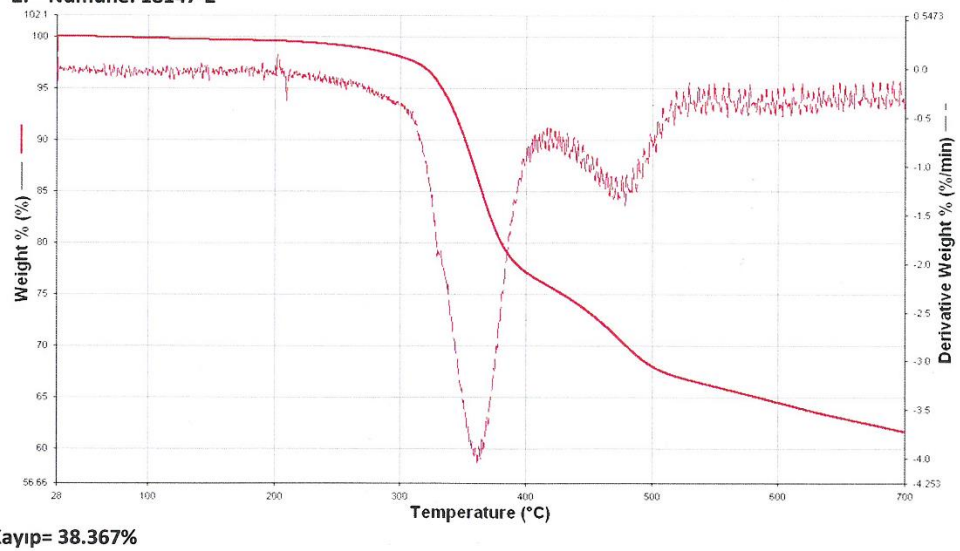


Figure 47. DSC Thermogram of P2.

1. Numune: 17148-1

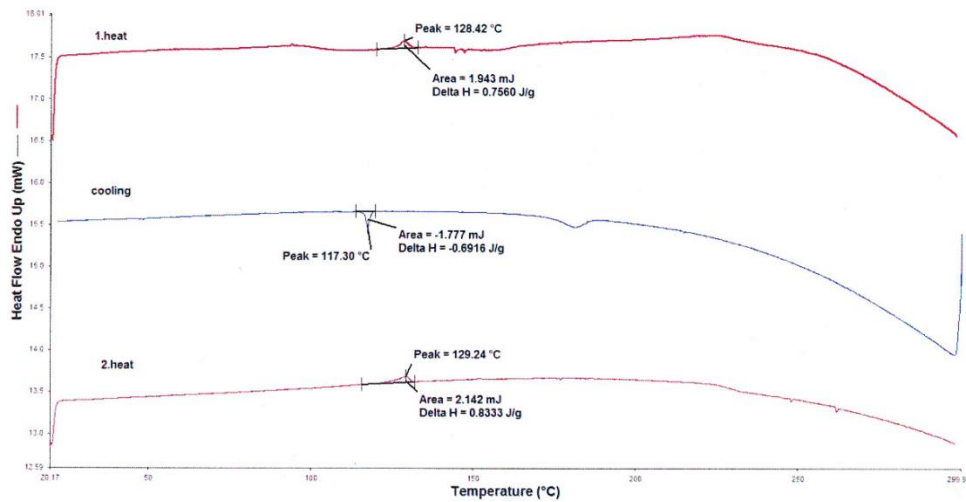


Figure 48. TGA Curve of P1.

2. Numune: 17148-2

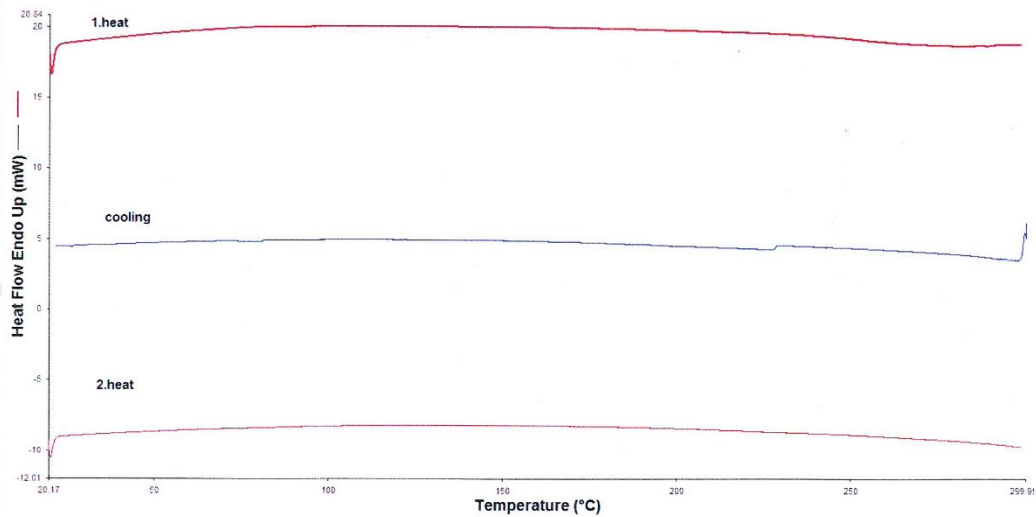


Figure 49. TGA Curve of P2.